ISTC Project # 3813

Phase relations in corium systems (PRECOS)

Annual Project Technical Report

on the work performed from 1.06. 2008 to 31.05. 2009
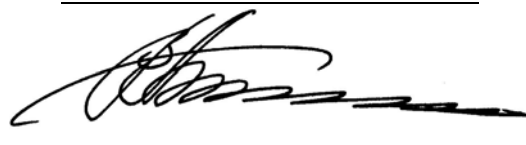
(First year)

Federal public unitary company "A.P. Alexandrov Research Institute of Technology" (FGUP NITI)

Project Manager	**Sevostyan V. Bechta** **Dr. Sci.**	
General Director	**Vyacheslav A. Vasilenko** **Dr. Sci., Prof.**	

February 2010

Title of the Project: **Phase relations in corium systems (PRECOS)**

Contracting Institute: Federal public unitary company "A.P. Alexandrov Research Institute of Technology" (FGUP NITI)

Participating Institutes: ITES OIVT RAS

Commencement Date: 01.06.2008

Duration: 36 months

Project Manager S.V. Bechta, Dr. Sci. Head of department, NITI

tel.: +7(813-69) 60 625

fax: +7(813-69) 23 961

e-mail: rital@sbor.net

1. Brief description of the work plan: objective, expected results, technical approach

Main Project objective is the experimental and theoretical studies of different compositions of the metal-oxidic U-Zr-O system and binary oxidic systems UO_2-SiO_2, UO_2-CaO, ZrO_2-FeO_x. Its goals: determine liquidus and solidus temperatures and tie lines in the miscibility gap, optimize available databases and verify numerical codes.

Experimental studies within the Project were performed on RASPLAV-3 and RASPLAV-4 setups. The method of induction melting in a cold crucible (IMCC) was used for producing melts having temperature levels up to 3300 K. The method has the following advantages:

− power deposition inside the melt;
− presence of crust between the melt and cold crucible wall, which prevents the crucible material mass transfer into the melt.

Combination of contact-free heating method and non-contaminating technique for melting oxides provides:

− melts having the purity not below the purity of initial components;
− considerable superheating of the melt above the liquidus temperature, also for chemically active oxidic materials;
− melting and long-term exposition of oxidic system in the molten condition both in the inert and in the oxidizing atmospheres;
− adjustable and compact melting unit.

RASPLAV-3,4 experimental facilities can produce up to 2 kg high-temperature corium in the inert and oxidizing atmospheres.

In the course of experiments solidus and liquidus temperatures were measured by the visual polythermal analysis in a cold crucible (VPA IMCC).

In the posttest analysis solidus and liquidus temperatures were evaluated using the following methods:

- visual polythermal analysis in the Galakhov microfurnace (VPA GM).
- differential thermal analysis (DTA).

The following methods were used in the physicochemical analysis of corium samples:
- X-ray fluorescence (XRF) and chemical analysis (ChA) – to determine elemental composition.
- X-ray diffractometry (XRD) and energy dispersion X-ray and (EDX) – to identify phase composition.
- Scanning electron microscopy (SEM) – to determine microstructure of samples.

2. Technical progress during the first year

In accordance with the experimental matrix the first two out of four tasks were planned for implementation during the first Project year. Both tasks are aimed at getting experimental and analytical data on the binary oxidic systems UO_2-SiO_2, UO_2-CaO, ZrO_2-FeO_x and metal-oxidic system U-Zr-Fe-O.

The tasks were defined in the following way:

Task 1   -   Investigation of various compositions of the metal-oxidic system aimed at determining T_{liq}, T_{sol} and tie-lines in the miscibility gap.
   Subtask 1.1 State of the art review.
   Subtask 1.2 Experimental investigations and analysis of produced data.

Task 2   -   Study of binary oxidic systems.
   Subtask 2.1 State of the art review.
   Subtask 2.2 Experimental investigations and analysis of produced data.

During the first Project year the following work has been completed.

Task 1   **Investigation of various compositions of the metal-oxidic system aimed at determining T_{liq}, T_{sol} and tie-lines in the miscibility gap.**

Subtask 1.1   State of the art review.

The published data have been found and analyzed. For further studies of the U-Zr-O system compositions in the U-ZrO_2 section have been recommended. Fig. 1.1. presents the numerical modeling of solidus and liquidus temperatures for this section, which was made using the GEMINI code and NUCLEA database.
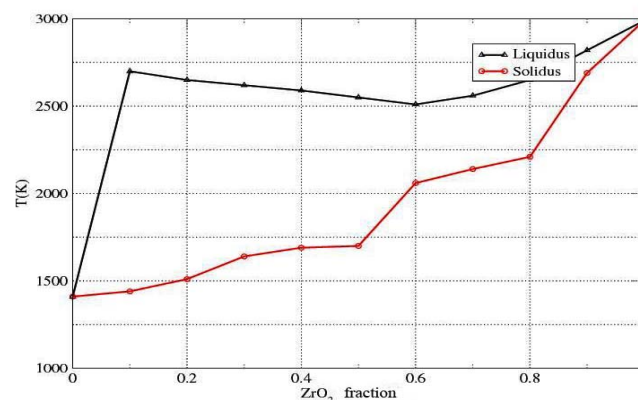

Fig. 1.1 – Liquidus and solidus temperatures in the U-ZrO_2 section

Subtask 1.2   Experimental investigations and analysis of produced data

In accordance with the approved Work Plan the studies of U-Zr-O system are carried out on the experimental facility with a pulse laser heating in the ITES OIVT RAS (Participating Institute 1), see Fig. 1.2. For the scoping tests specimens having thermophysical characteristics similar to materials studied within the work program were used.
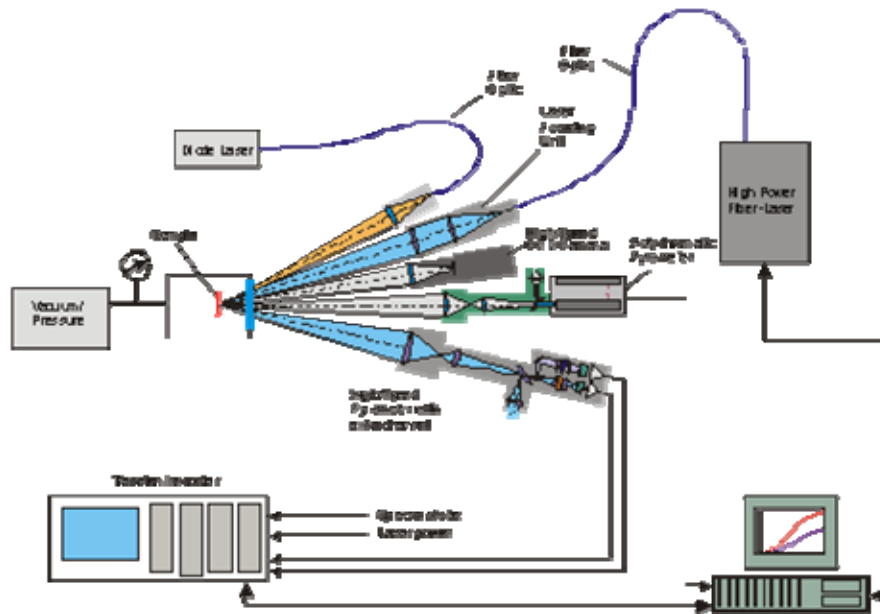

Fig. 1.2 – Setup schematics

The following activities have been performed:

- a system was established for controlling the laser output power, which has the programmed pulse and time resolution of 1 ms;
- a special focusing system was manufactured;
- a system was tested, which registers phase transitions by changes in reflection characteristics using the lighting laser;
- a multi-channel fast-response pyrometer was manufactured;
- the hardware-software system was put into operation, which eliminates the laser power instability in the first stage of pulse generation (approx. 200 ms after turning on);
- a program for numerical modeling of two-component materials behavior at the impact of surface laser heating. The mathematical model is based on the assumption about the existence of a local thermodynamical equilibrium in all points of the studied material and on the equations of the energy and mass transfer of the two components. The results of calculations enable to interpret dynamics of the phenomena taking place inside the specimen during its heating and cooling, which cannot be studied directly by experiments.

Additional equipment was acquired using extra-budgetary resources. Certain components were manufactured, tested and calibrated, in particular:

- A multichannel (256 optical channels) fast-response pyrometer was produced, its optical system was tuned, nonlinearity was checked and adjusted, it was calibrated by wavelengths. Software was developed for high-speed data transfer to PC directly and for the synchronization with the laser system.
- The high-temperature (up to 3000 K) model of an absolutely black body was developed for the calibration of multichannel pyrometer.
- A VideoScan camera for high-speed recording was installed; it makes it possible to monitor the specimen surface in the laser heating zone at the speed of 500 frames per minute with a spatial resolution of 1200 x1000 pxls and amplitude resolution up to 10 bit.

In the scoping tests ceramic specimens were used, which were made from the suboxidized Fe-Zr-O system in the IVTRAN. There were two kinds of specimens: sintered and compacted (without additional annealing). In the scoping tests all systems in the experimental setup were tuned and adjusted and a possibility for experiments with specimens made only by the powder compaction was clarified. It was found that at laser heating the behavior of compacted specimens has no principal difference from the behavior of samples produced by melting or sintering (Fig. 1.4). Fig. 1.3 shows a specimen cut from the ingot, which was molted using the IMCC technique in the experiment of Project #1950b ISTC (CORPHAD).
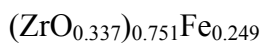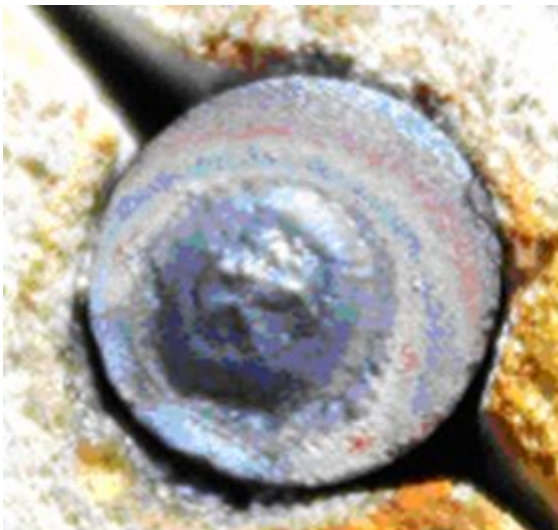

$(ZrO_{0.337})_{0.751}Fe_{0.249}$

Fig. 1.3 - Specimen cut out from ingot of CORPHAD test
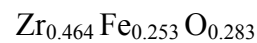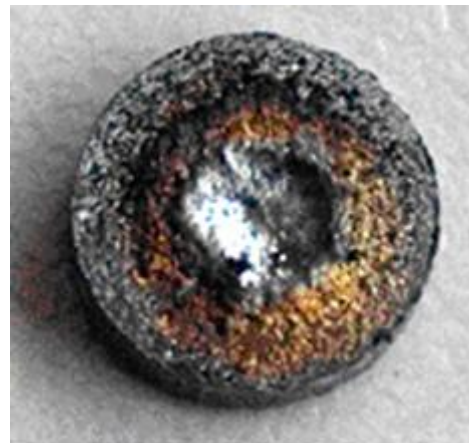

$Zr_{0.464}Fe_{0.253}O_{0.283}$

Fig. 1.4- Compacted sample

The Zr-O system was chosen as a model for refining the experimental methodology. A set of specimens having different Zr-O ratios was made in the OIVT RAS in the reducing vacuum furnace (Table 1.1).

Table 1.1 – Specimens for the studies of the Zr-O phase diagram produced by OIVT RAS

Composition	Porosity, %
$ZrO_{0.094}$	3
$ZrO_{0.11}$	3
$ZrO_{0,157}$	11
$ZrO_{0.31}$	27
$ZrO_{0.64}$	29
$ZrO_{1,415}$	17
$ZrO_{1,57}$	12
$ZrO_{1,62}$	18
$ZrO_{1,65}$	13

Measured liquidus temperatures for the Zr-O system are shown in Fig. 1.5 in comparison with the known phase diagram.
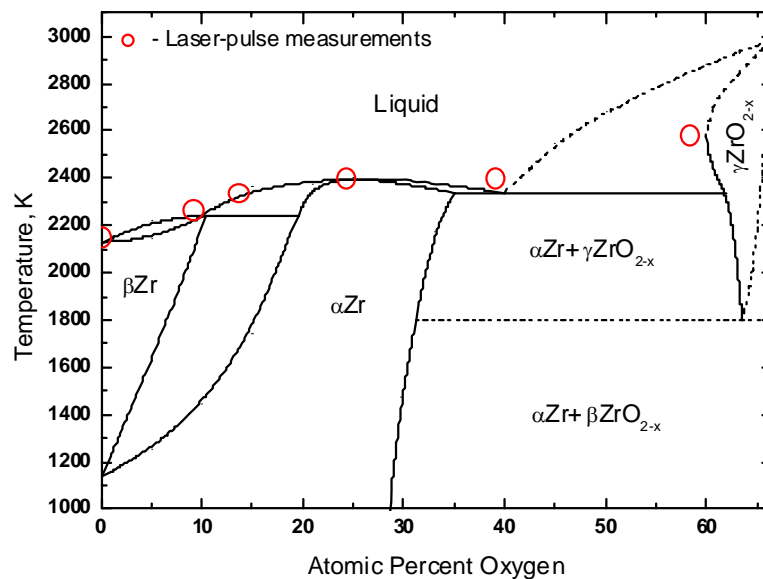

Fig. 1.5 – Measured data of the Zr-O system

Fig 1.5 shows a rather good convergence of measurements and published data. But the temperature measured in the point, which approximately corresponds to 58 at.% oxygen, has a distinct difference from solidus temperature and from the hypothetical liquidus line. Additional experiments are necessary to clarify this issue. Note that location of this point is important for studying the Zr-U-O diagram within the project (see Fig. 1.6).
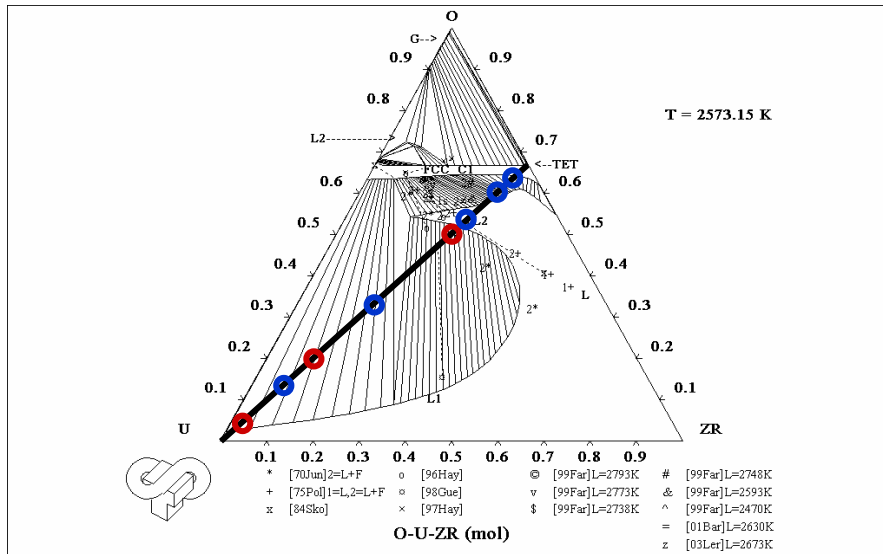
Fig. 1.6 – Diagram of the Zr-U-O system

Diagram of the Zr-U-O system (ZrO_2-U section) shows points, which correspond to the compositions planned for future experiments. It follows from Fig. 1.6 that a better understanding of the phase diagram of a ternary system requires both the study of ZrO_2-U section and data on the behavior of binary nonstoichiometric systems: Zr-ZrO_2 and U-UO_2. The last-mentioned system is planned for studies within the project.

NPO "Lutch" has developed a hydride technology and made a synthesis of specimens (red dots on the diagram of Fig. 1.6) having compositions present in the mentioned U-ZrO_2 section of the U-Zr-O system. Characteristics of the synthesized specimens belonging to the first two batches are given in Table 1.2, Fig. 1.7 shows microstructure of one of the synthesized specimens.

Table 1.2 – Characteristics of the synthesized specimens

| Batch (No if items.)	Size of tablets, mm	Composition, mass.%	Charge for synthesis	Chemical analysis, mass.%.	Phase composition
1 (10)	D=8,8±0,1 h=3,0±0,2	U-65,9 ZrO_2 -34,1	UO_2 $ZrH_{1,9}$.	U - 65.82	Solid solution based on UO_2 (a = 5,456 Å); Solid solution of oxygen in α-Zr (α-Zr(O)) (a = 3,25 Å; c = 5,20 Å); Solid solution based on. α-U (a = 2,85 Å; b = 5,86 Å; c = 4,96 Å); Average grain size- <20 μm
2 (10)		U-98,9 ZrO_2 -1,1	UH_3 ZrO_2	U - 98.67	Solid solution based on α – U (a = 2.86 Å; b = 5.87 Å; c = 4.96 Å); Solid solution based on UO_2 (a = 5.46 Å); average grain size- <10 μm
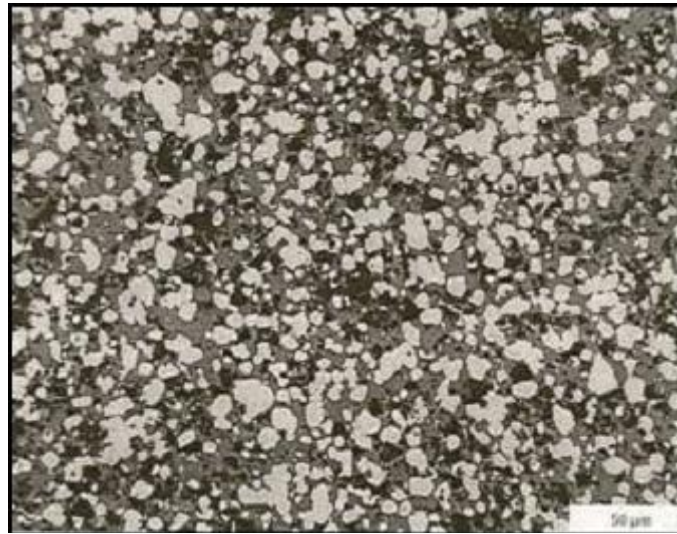
Fig. 1.7 – Microstructure of synthesized specimen

One of the objectives in the Zr-O investigation was to adjust the method of laser pulse heating for studying compositions with a high content of metal (up to pure Zr). In the last case the high heat conductivity of the material, low absorption coefficient of laser radiation (and a correspondingly high reflection coefficient) explain the application of higher laser power and the necessity to protect the optical monitoring system from a strong reflected laser radiation.

For the first time OIVT RAS used a high-speed CMOS camera, which can make about 1000 frames/s and has a spatial resolution of about 1000x1000. This enabled to visualize the processes of melting and crystallization. The high-speed video recording was carried out in the mode of the specimen self-lighting (it enabled to evaluate the radial temperature gradients in the melt) and in the mode of specimen surface lighting by laser at the 503 nm wavelength, (it enabled to monitor phenomena taking place on the surface). For example, the video recording of the surface with its lighting enabled to follow the melt boundary dynamics and compare it with the data provided by the 2D models of temperature fields.
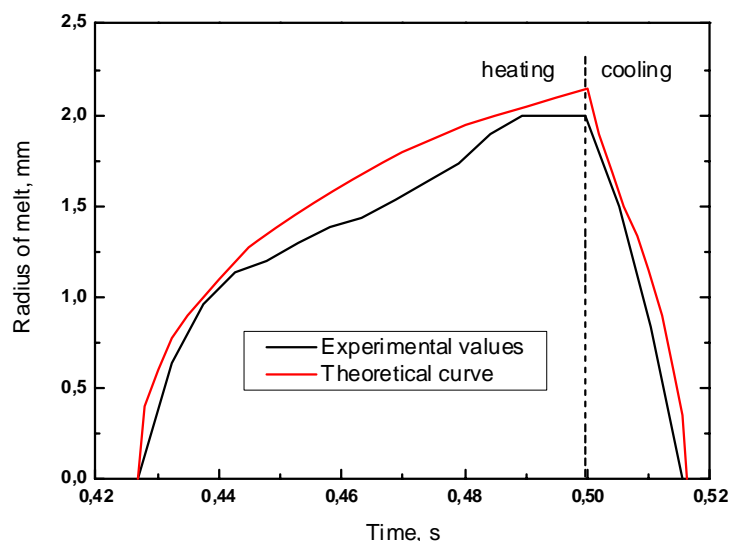

Fig. 1.8 – Comparison of the experimentally measured diameter of the zirconium melt boundary and the numerical model

Fig. 1.8 shows a comparison between the experimentally measured Zr melt boundary and the data of mathematical modeling. It is evident that measured and calculated data agree well, taking into account real experimental conditions and possible measurement errors.

Task 2 Study of the binary oxidic systems.

Subtask 2.1 State of the art review.

UO_2-SiO_2 system

Topical publications were found and analyzed. Figs. 2.1 and 2.2 show the published phase equilibria in the system; they have considerable differences. In one case it is simple phase equilibria with eutectics, another has both eutectics and miscibility gap. The CORPHAD studies presented in Fig. 2.3 confirm the presence of a miscibility gap. First CORPHAD data indicate higher temperature boundaries of the gap than Lungu diagram, but these results will have to be confirmed.
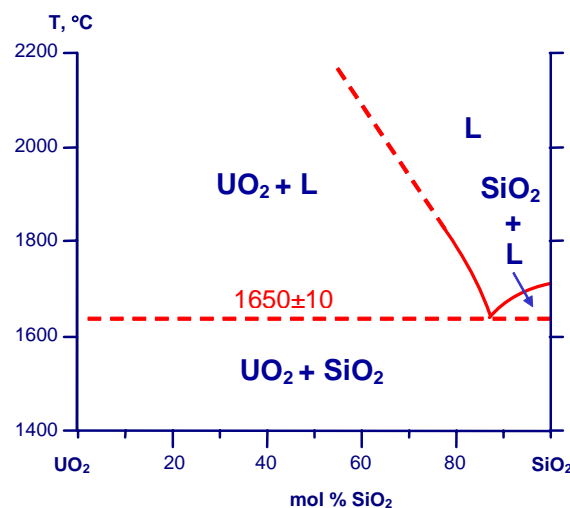

Fig. 2.1 - UO_2–SiO_2 phase diagram with an eutectic by S.M. Lang et al., Nat. Bur. Stand., Circular 568. 1956. Eutectic composition (15-10) UO_2 – (85-90) SiO_2, mol %. Eutectic temperature 1650±10 °C
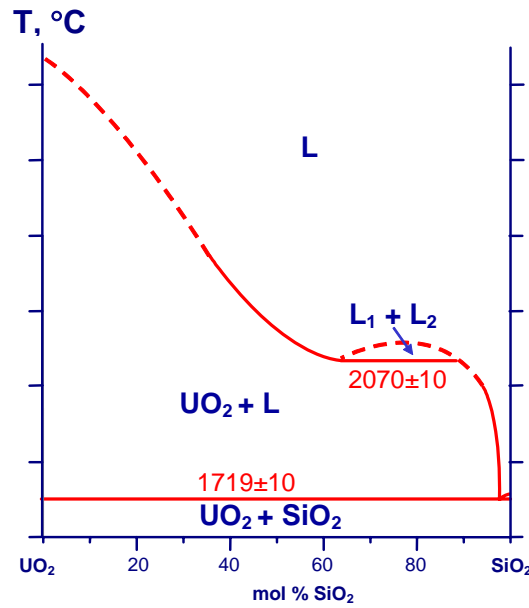
Fig. 2.2 - Fusion diagram with the miscibility gap by S. Lungu, Romanian J. of Physics. 1962. V. 7. N 4. P. 419. Eutectics composition: 2 UO₂ – 98 SiO₂, mol %. Eutectic temperature 1719±10 °C. Monotectic temperature 2070±10 °C
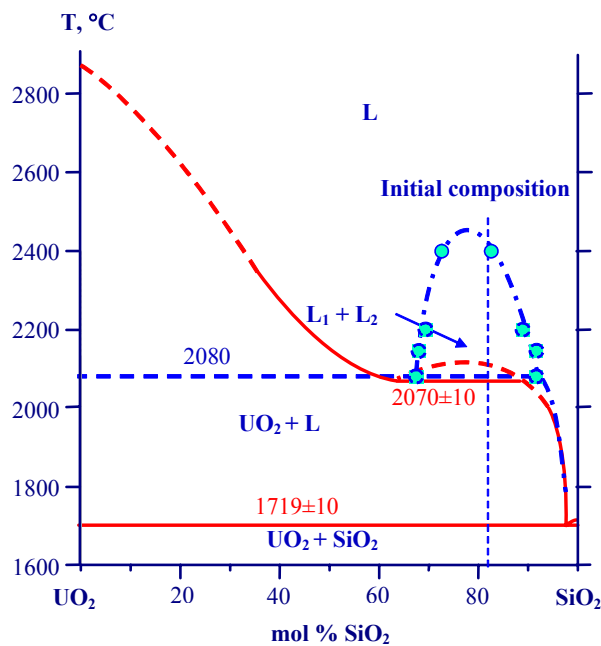

Fig. 2.3 - Red lines – Lungu diagram. Blue lines and blue points – results of our previous work within the CORPHAD project

ZrO₂-FeOₓ system

Analysis of publications on the phase equilibria in the ZrO₂-FeOₓ systems showed that the data were quite limited [2-4]. In the analyzed sources the data on the position of phase equilibria lines and on the phase diagram characteristics have a divergence. Reference [1] in subsection 2.2

Data disparity on the FeOₓ solubility in the solid ZrO₂-based phases found in the mentioned publications requires a special attention both to the posttest analysis and specimen

preparation. Depending on a method of synthesis we can get ZrO_2-based solid solution having different contents of the second component [5]. In a component based on the element having different oxidation degrees differently charged iron ions can localize in the ZrO_2 lattice; this depends on the conditions, in which solid solutions were produced.

UO_2-CaO system

      Publications were found and analyzed.

      Comparison of UO_2-CaO phase diagrams, which belong to different authors (Fig. 2.4) shows a different position of the eutectic point both in terms of composition and temperature. Different solubility of CaO in UO_2 should also be noted

      The analysis of available information on phase equilibria in the UO_2-CaO system has proven the necessity to specify the composition and temperature of the eutectic point, as well as the solubility of CaO in UO_2; liquidus temperatures in the UO_2 and CaO-enriched domains should also be evaluated.
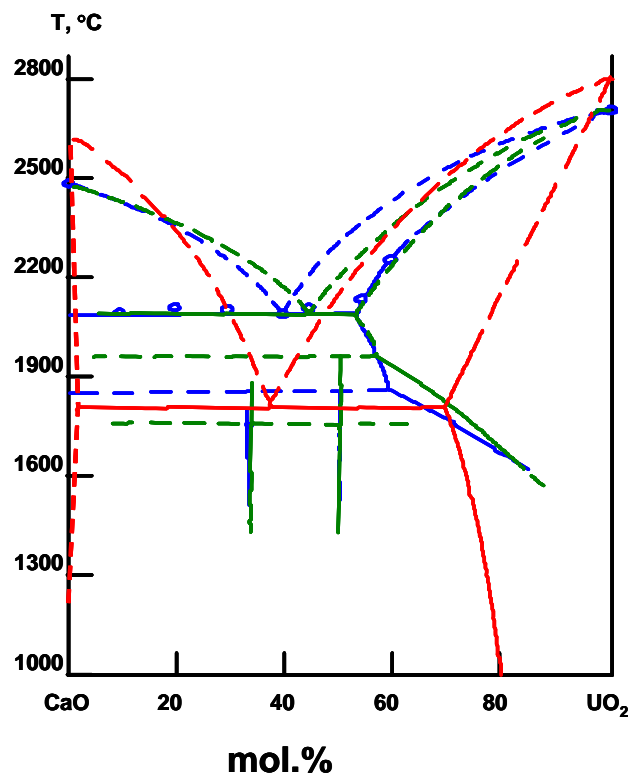
Blue line [5]; Green line [6]; Red line [7].

Fig. 2.4 – Versions of the UO_2-CaO phase diagram

**Subtask 2.2   Experiments and experimental data analysis.**

UO_2-SiO_2 system

      During the reported period special efforts were directed at specifying position of the liquidus line in the system from the UO_2 side.

      The binary oxidic system UO_2-SiO_2 was studied by the VPA IMCC method (experiments of the PRS series), high-temperature specimen annealing in the Galakhov

microfurnace was followed by their quenching (experiments of the GPRS series) and by SEM/EDX.

Experiments PRS1-3, 8 were conducted on the RASPLAV-4 test facility. Its schematics is given in Fig. 2.5.
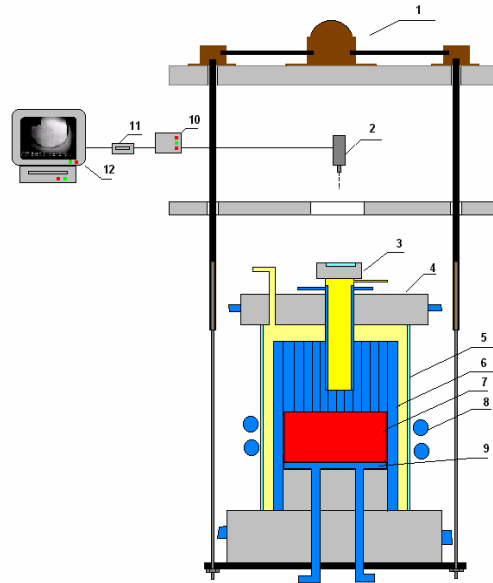
1 – drover for vertical shift of the crucible 2 – pyrometer combined with video camera;
3 – pyrometer shaft; 4– water-cooled cover; 5 – quartz tube; 6 – crucible section; 7 - RASPLAV;
8 - inductor; 9 – bottom calorimeter; 10 – data acquisition system; 11 – device for inserting measured values into video frames; 12 – monitor/video recorder.

Fig. 2.5 - RASPLAV-4 schematics

Experimental matrix of completed PRS series for the UO_2-SiO_2 system is presented in Table 2.1.

Table 2.1 – Experimental matrix of PRS series for the UO_2-SiO_2 system

Test	Content, mass.% / at.%	
	UO_2	SiO_2
PRS1	80 / 47	20 / 53
PRS2*	75 / 40	25 / 60
PRS3	85 / 56	15 / 44
	90 / 67	10 / 33
PRS8*	75 / 40	25 / 60
	66 / 30	34 / 70
	60 / 25	40 / 75

* - Compositions of two experiments in the PRS series (2 and 8(I)) are the same.

Liquidus temperature measured in experiments PRS 1-8 was specified in the small-scale experiments GPRS1,4,5-13, in which the mixture melting was followed by its quenching in molybdenum crucibles. GPRS test were conducted using the innovative experimental facility, the Galakhov microfurnace [1] developed and manufactured in the Grebenschikov ISCh RAS and modified by NITI (Fig. 2.6).
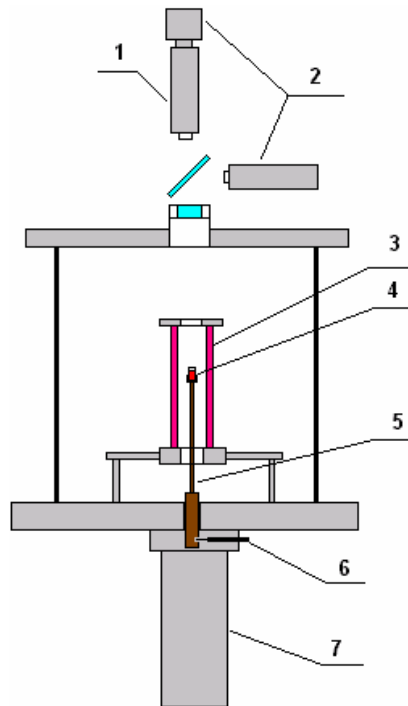
1 –pyrometer; 2- video cameras; 3 -W – tubular heater; 4- molybdenum crucible;5-
molybdenum specimen holder; 6- electromagnetic lock;7 –specimen quenching chamber.

Fig. 2.6 – Schematics if modernized Galakhov microfurnace

Table 2.2 shows the experimental matrix of GPRS series in the UO_2-SiO_2 system

Table 2.2 – Experimental matrix if the GPRS series. The UO_2-SiO_2 system

Test	Content, mass.% / at.%		Temperature of crucible heating, °C	Exposition time, s
	UO_2	SiO_2		
GPRS1			2050	5
GPRS2	50.7 / 18.6	49.3 / 81.4	2080	5
GPRS3			2080	10
GPRS4	80 / 47	20 / 53	2500	
GPRS5			2200	
GPRS6	80 / 47	20 / 53	2300	
GPRS7*			2400	
GPRS8			2220	
GPRS9	75 / 40	25 / 60	2300	1
GPRS10			2100	
GPRS11			2300	
GPRS12	85 / 56	15 / 44	2400	
GPRS13			2500	
GPRS14	80 / 47	20 / 53	2400	

* - experiment failed, was repeated and labeled as GPRS14.

- **Experiment PRS1**

In PRS1 three T_{liq} measurements were made by VPA IMCC; three melt samples were taken to determine the melt composition. Fig. 2.7 shows pyrometer readings and anode voltage dynamics during the experiment. Fig. 2.8 shows a thermogram fragment at the moment of T_{liq} measurement.
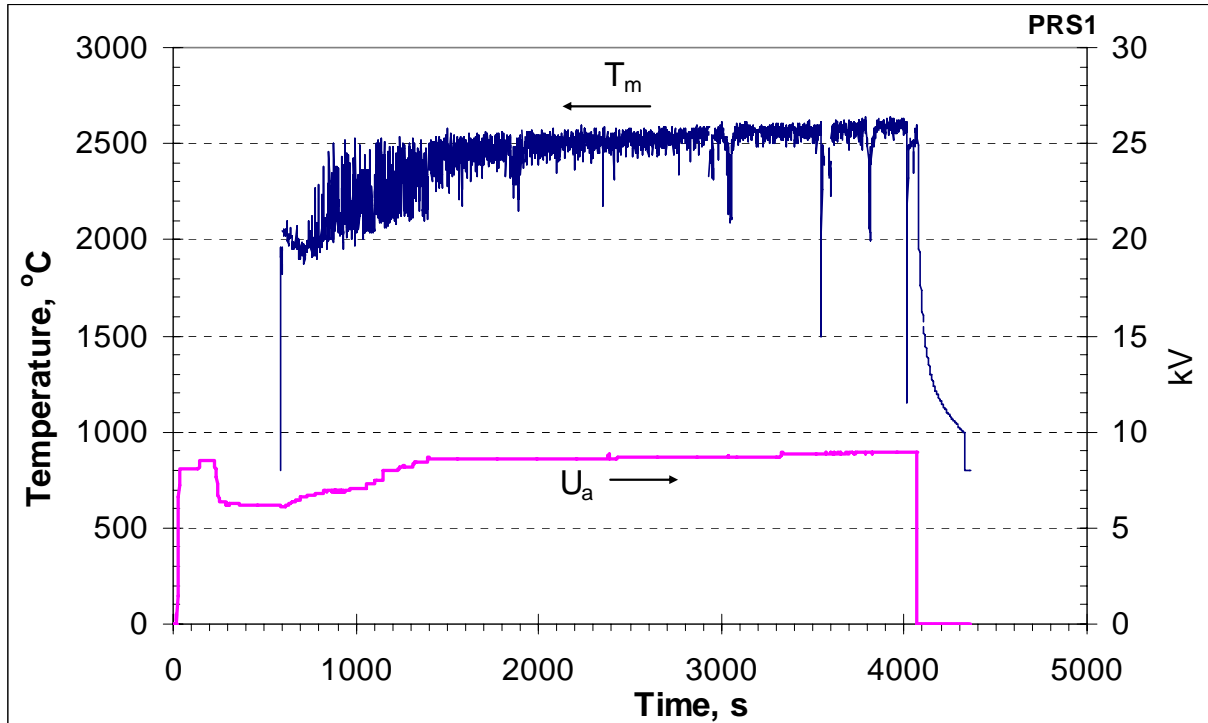

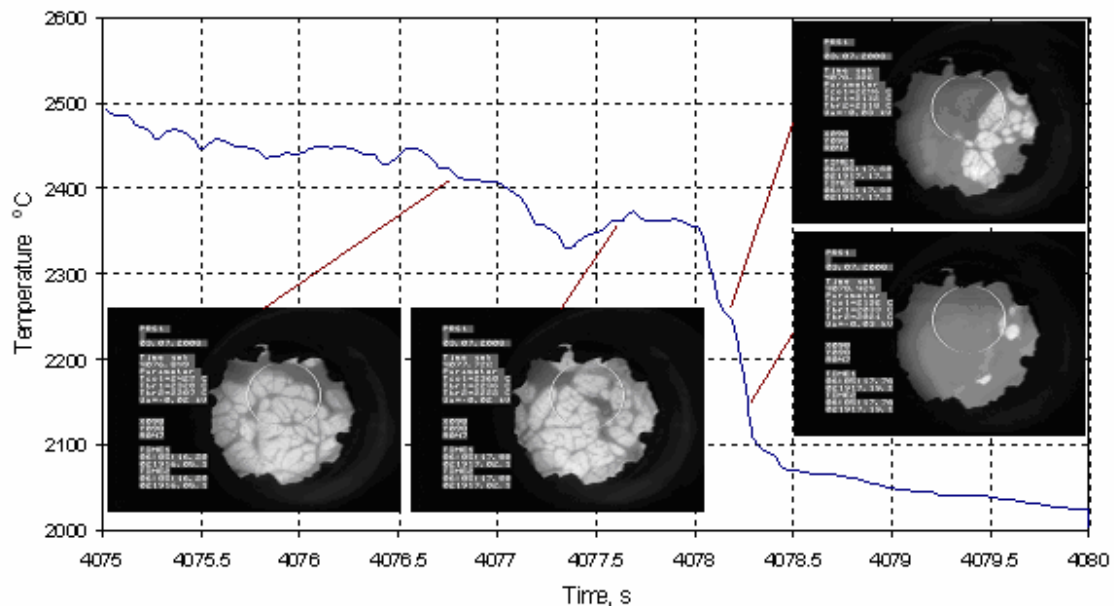**Fig. 2.7 – Anode voltage dynamics (U_a) and pyrometer readings (T_m)**

Fig. 2.8 - PRS1 thermogram fragment

Liquidus temperatures measured in the experiment: 2425, 2400, 2380°C.

- **Experiment PRS2**

In PRS2 three T_{liq} measurements were made by VPA IMCC; three melt samples were taken to determine the melt composition. Fig. 2.9 shows pyrometer readings and anode voltage dynamics during the experiment. Figs. 2.10-2.12 show thermogram fragments at the moment of T_{liq} measurement..
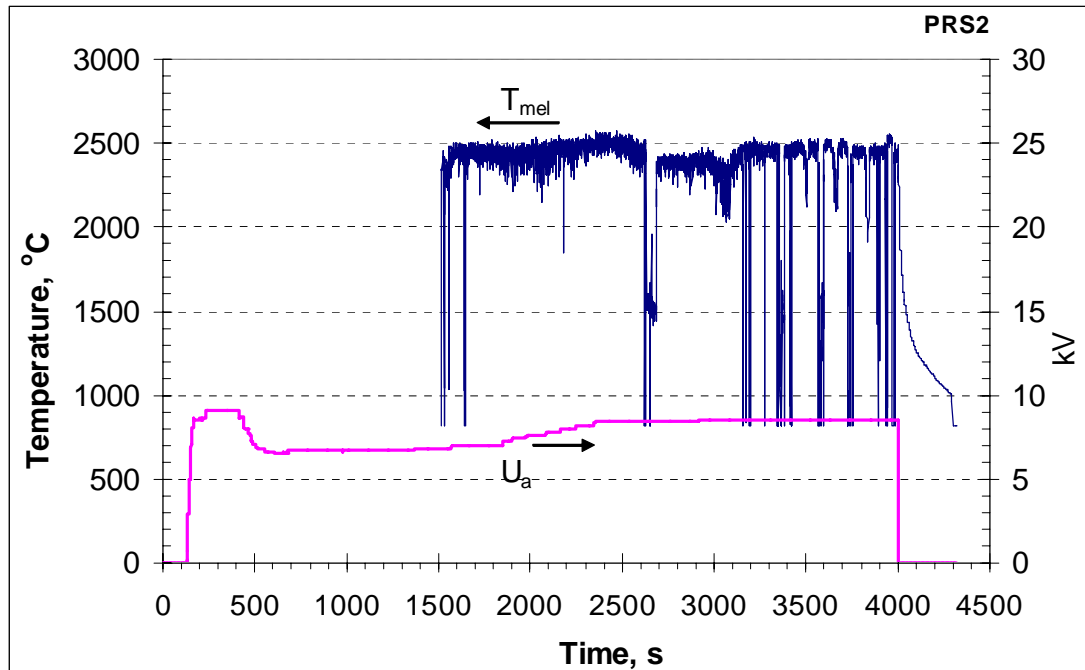

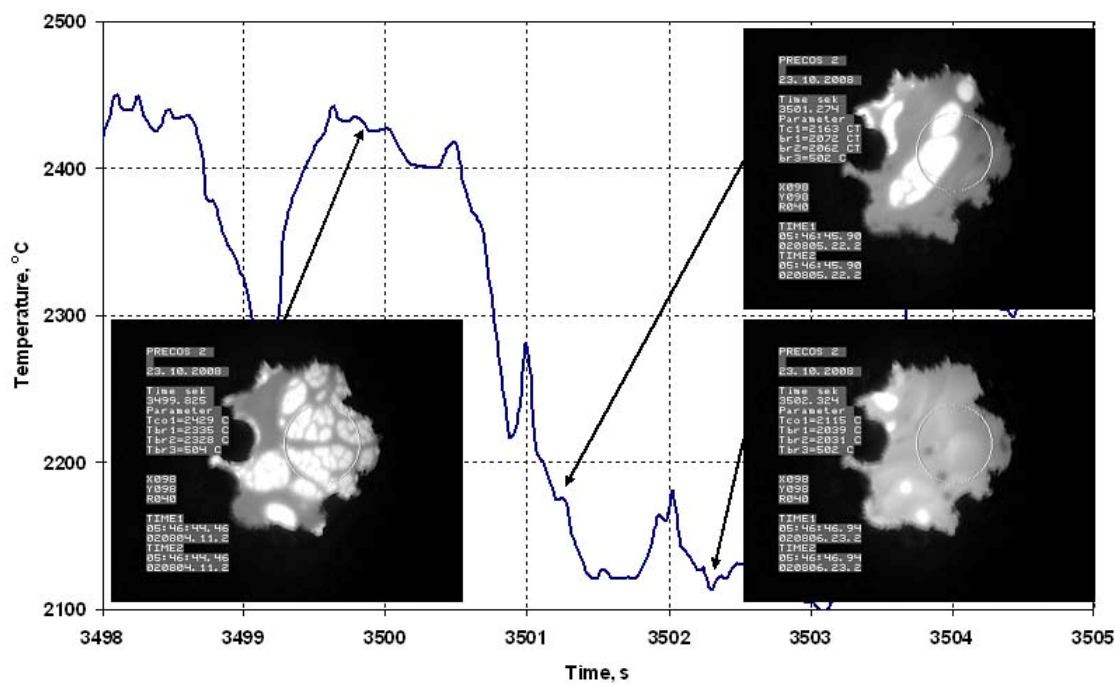**Fig. 2.9 - Anode voltage dynamics (U_a) and pyrometer readings (T_m)**

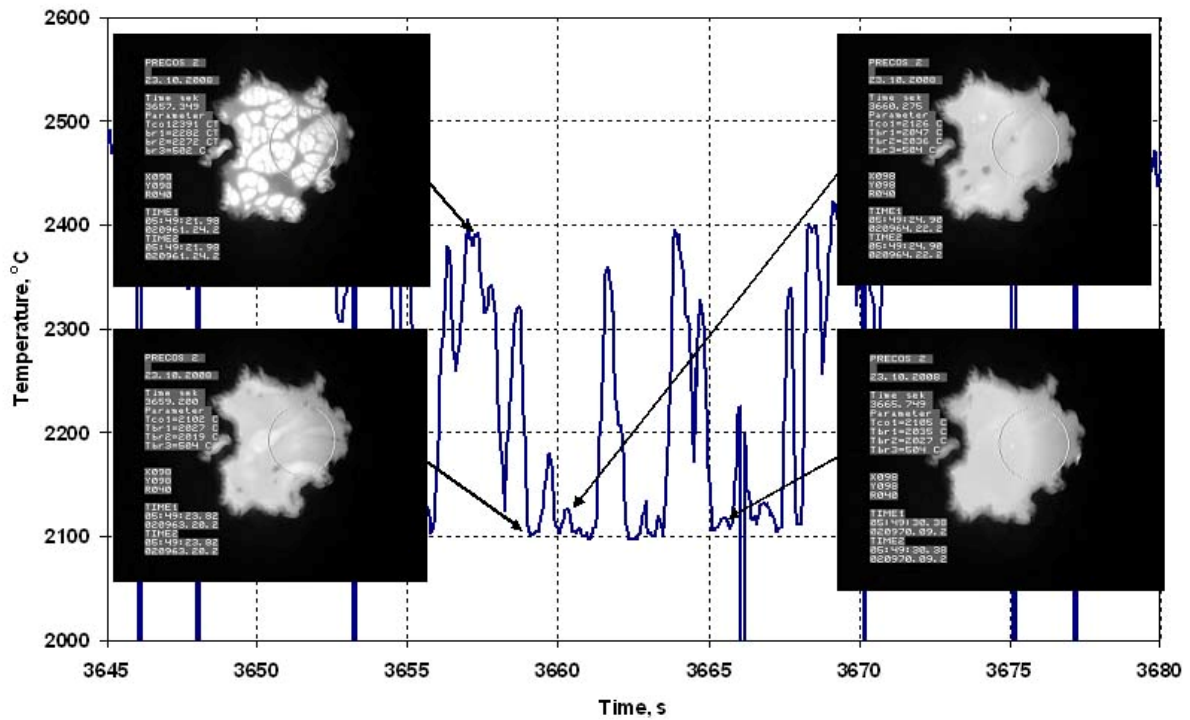**Fig. 2.10 – Thermogram fragment, experiment PRS2**

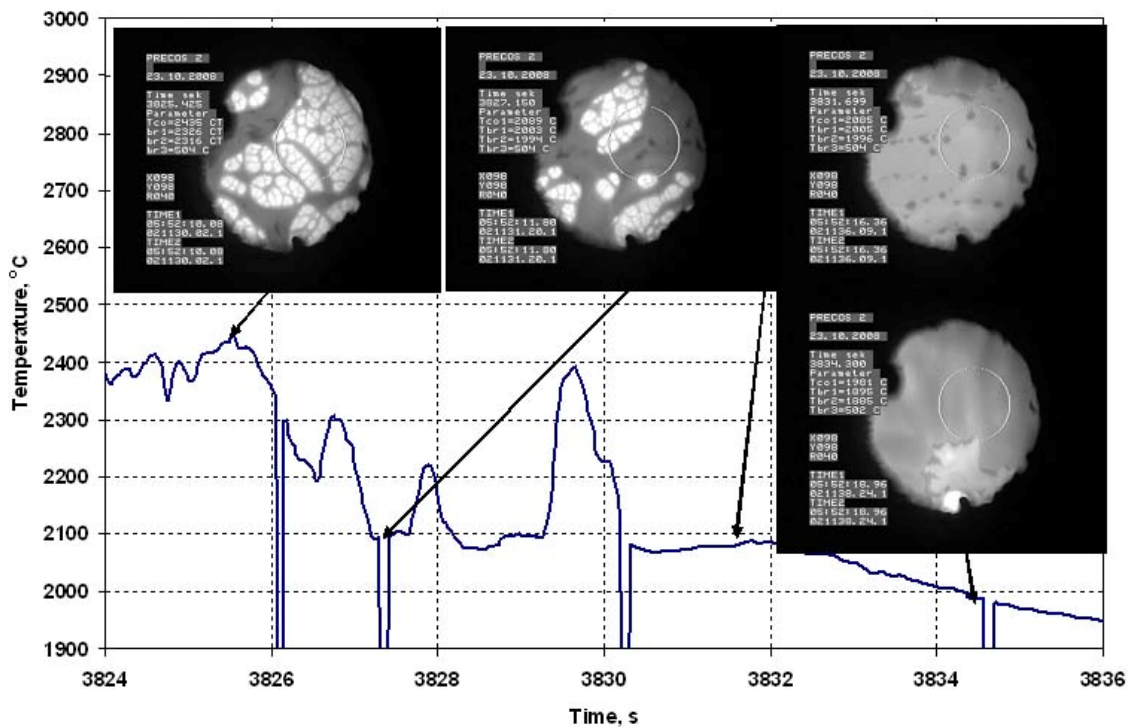**Fig. 2.11 - Thermogram fragment, experiment PRS2**

Fig. 2.12 - Thermogram fragment, experiment PRS2

Liquidus temperatures measured in PRS2: 2100, 2085, 2060°C, respectively.

- **Experiment PRS3**

In PRS3 two melt compositions were studied (Table 2.1). Two compositions were produced during one melting session by adding UO_2 into the molten pool. Fig. 2.13 shows pyrometer readings and changes in the anode voltage during the experiment. In PRS3 two T_{liq} measurements were made by VPA IMCC; two melt samples were taken to identify the first melt composition; three other samples were taken and three T_{liq} measurements were made after the UO_2 addition. Figs.2.14-2.18 show thermogram fragments at the moment of liquidus temperature measurement.
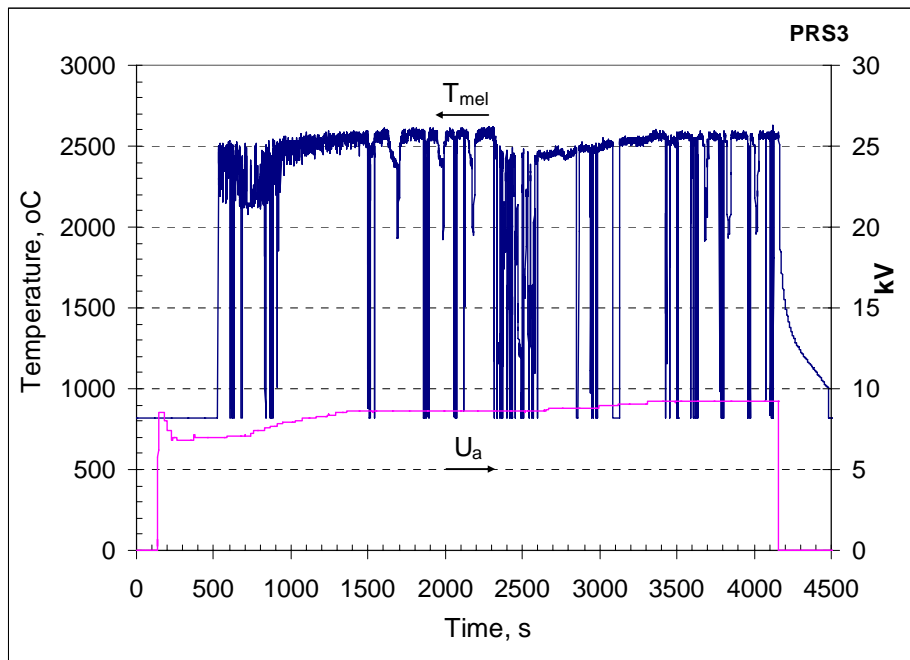

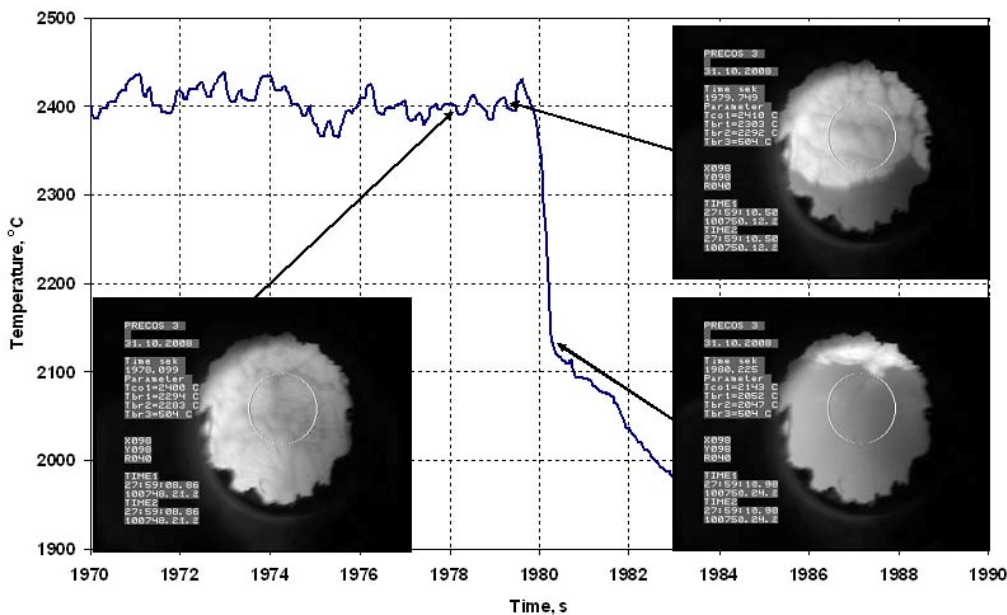**Fig. 2.13 - Anode voltage dynamics (U_a) and pyrometer readings (T_m)**

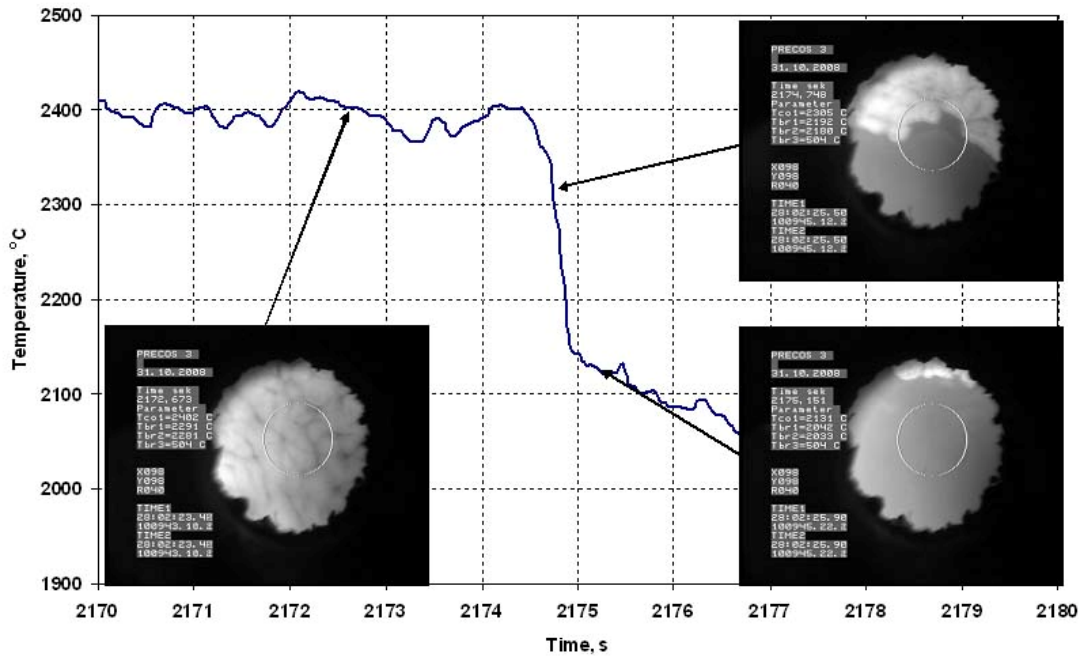**Fig. 2.14 - Thermogram fragment, experiment PRS3**

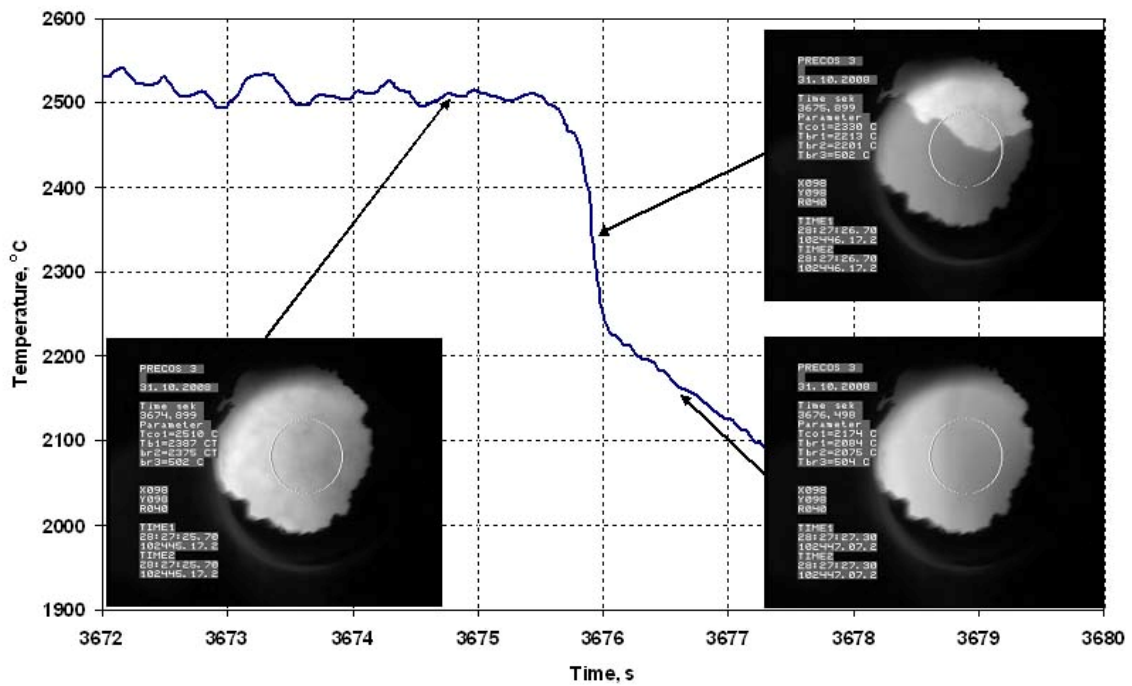**Fig. 2.15 - Thermogram fragment, experiment PRS3**

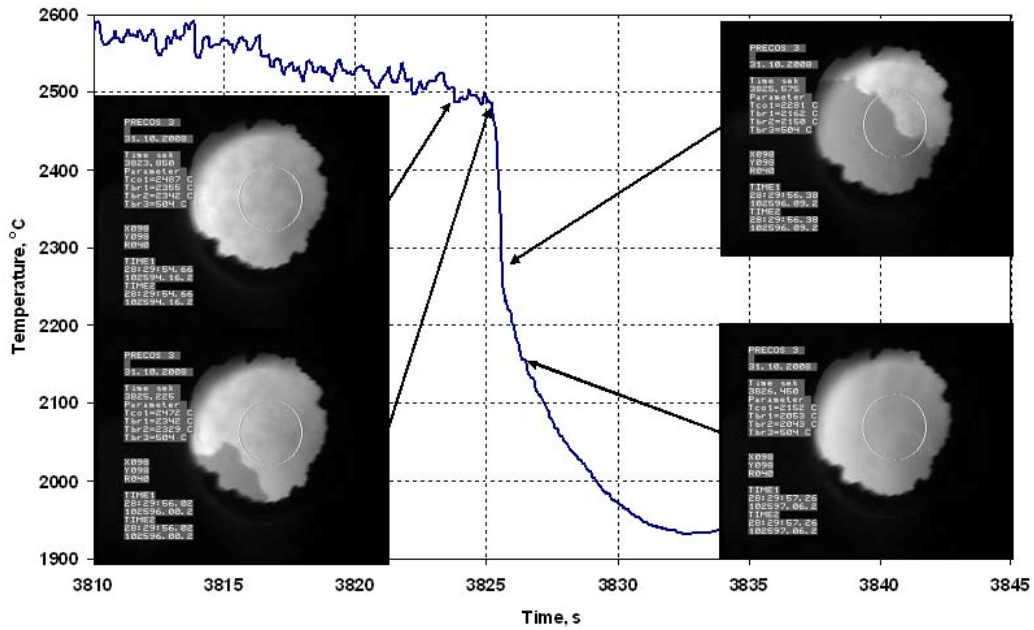**Fig. 2.16 - Thermogram fragment, experiment PRS3**

Fig. 2.17 - Thermogram fragment, experiment PRS3
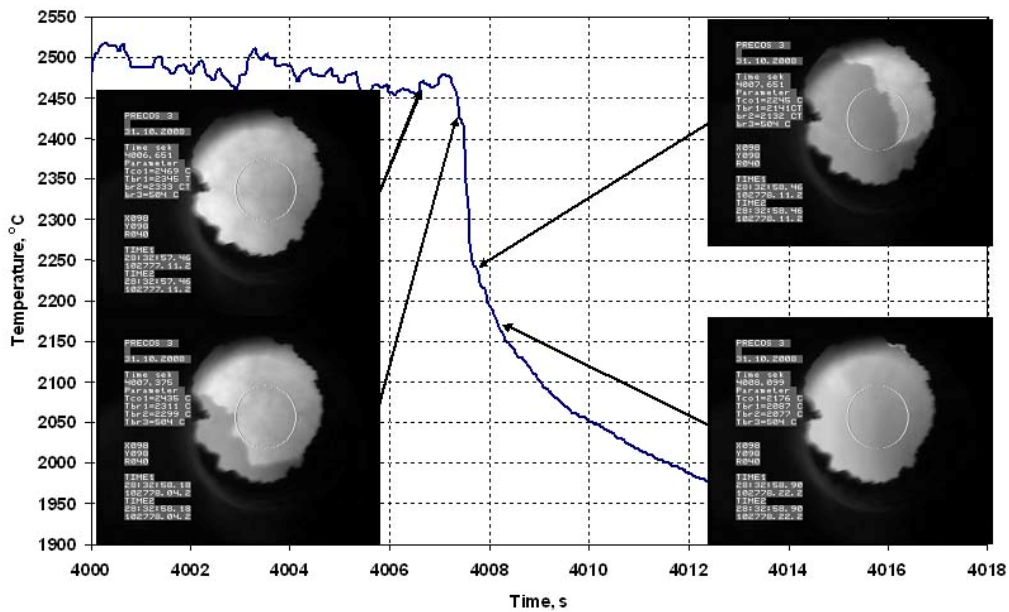
Fig. 2.18 - Thermogram fragment, experiment PRS3

Measured liquidus temperatures for the first composition are 2400, 2402°C, respectively. For the second composition they are 2487, 2469 and 2492°C.

- **Experiment PRS8**

Experiment PRS8 was performed to clarify the melt crystallization character in and beyond the miscibility gap in the IMCC conditions.

Experiment PRS8 studied three melt compositions. Two last compositions were produced during one melting session by adding SiO_2 into the molten pool. Fig. 2.19 shows pyrometer readings and anode voltage dynamics in the course of experiment.
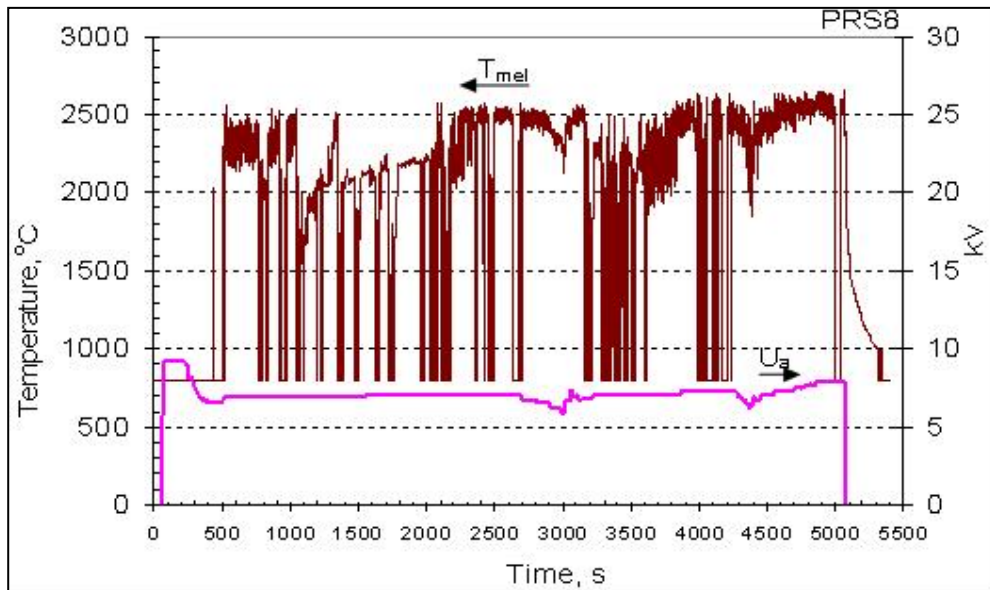
Fig. 2.19 - Anode voltage dynamics (U_a) and pyrometer readings (T_m)

After adding the second batch of SiO_2 into the melt a principal change in the flow and in the convective pattern in the melt surface was registered (see Fig. 2.20).
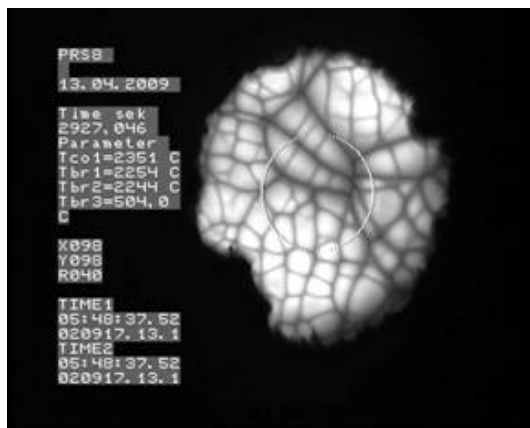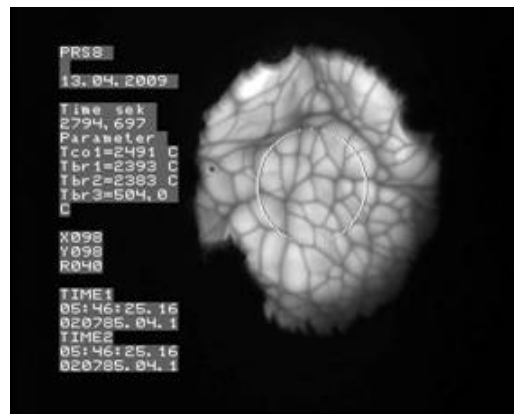
2351s   **2794s**

a)
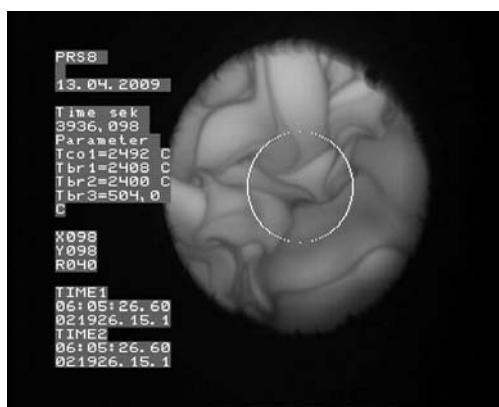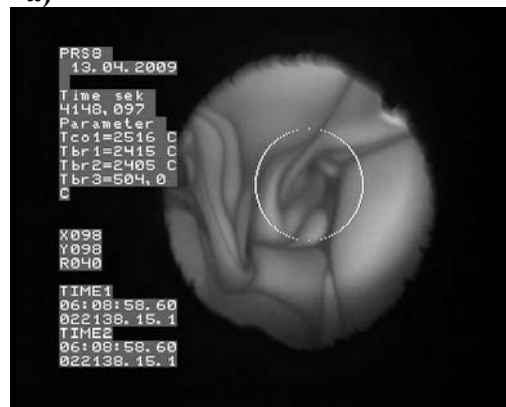
3936s   **4148s**

b)

Fig. 2.20 – Molten pool surface
a)- after adding the first portion of SiO_2; б)- after adding the second portion of SiO_2

In the course of PRS8 probe samples of different melt compositions were taken both within and beyond the hypothetical miscibility gap boundaries.

Table 2.3 shows measured melt compositions of samples taken during the liquidus temperature measurements in all conducted experiments.

Table 2.3 – Measured melt compositions

| Experiment	Position	Content recalculated for oxides, mol.%	
		UO_2	SiO_2*
PRS-1	*Sample #1** *	*46.02±3.0*	*53.98*
	Sample #2	58.63±4.1	41.37
	Sample #3	59.85±4.3	40.15
PRS-2	Sample #1	42.73±2.8	57.27
	Sample #2	43.69±2.8	56.31
	Sample #3	37.36±2.4	62.64
PRS-3	Sample #1	59.36±4.2	40.64
	Sample #2	59.36±4.2	40.64
	*Sample #3** *	*60.81±4.4*	*39.19*
	Sample #4	66.60±4.9	33.40
	Sample #5	70.07±5.3	29.93

Notes:
*- from residue;
**- data are in conflict with the general tendency. They are excluded from Table 2.4

Fig. 2.21 presents all liquidus temperatures of the binary UO_2-SiO_2 system measured during the reported period
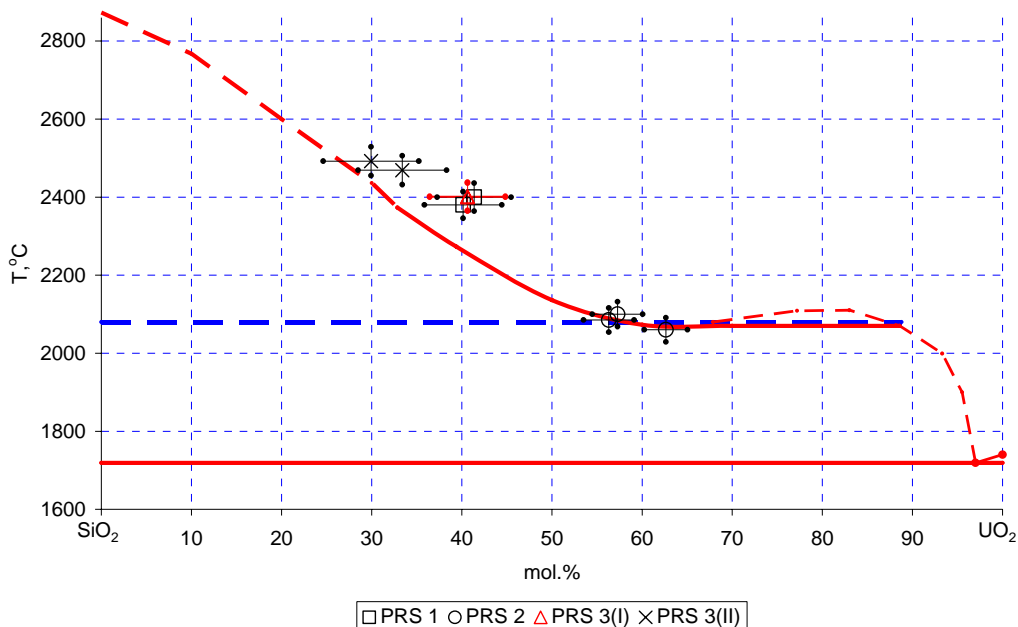

Fig. 2. 21 – Phase diagram of the UO_2- SiO_2 system

Some experimental points are located at a distance from the liquidus line. The completed integrated analysis of these points revealed some deficiencies in the chemical

analysis. Table 2.4 gives the checked experimental data on liquidus temperatures of different compositions.

Table 2.4 – Checked and recommended liquidus temperatures of PRS1-3 melt compositions

Experiment	Content, mol.%		T_{liq}, °C
	UO_2	SiO_2	
PRS1	58.63±4.1	41.37	2400±36
PRS1	59.85±4.3	40.15	2300±34
PRS2	42.73±2.8	57.27	2100±32
PRS2	43.69±2.8	56.31	2085±31
PRS2	37.36±2.4	62.64	2060±31
PRS3 (I)	59.36±4.2	40.64	2400±36
PRS3 (I)	59.36±4.2	40.64	2402±36
PRS3 (II)	66.60±4.9	33.40	2469±37
PRS3 (II)	70.07±5.3	29.93	2492±37

Results of all completed experiments have been analyzed and a program of further studies aimed at specifying miscibility gap boundaries and liquidus line position has been defined.

- **Experiments GPRS 1-3**

In order to specify the miscibility gap boundaries and temperature of monotectic transformation, the isothermal annealing of mixtures in molybdenum crucibles inside the Galakhov microfurnace was performed. Table 2.2 gives the annealing characteristics. Fig. 2.22 shows the microphotographs of GPRS1-3 polished sections.

After annealing the crucibles were cut along the axis and used for making templates. The resulting specimens were subjected to SEM-EDX analysis.

GPRS 1   **GPRS 2**   **GPRS 3**

2050°C, 5 min.   **2080°C, 5 min.**   **2080°C, 10 min.**
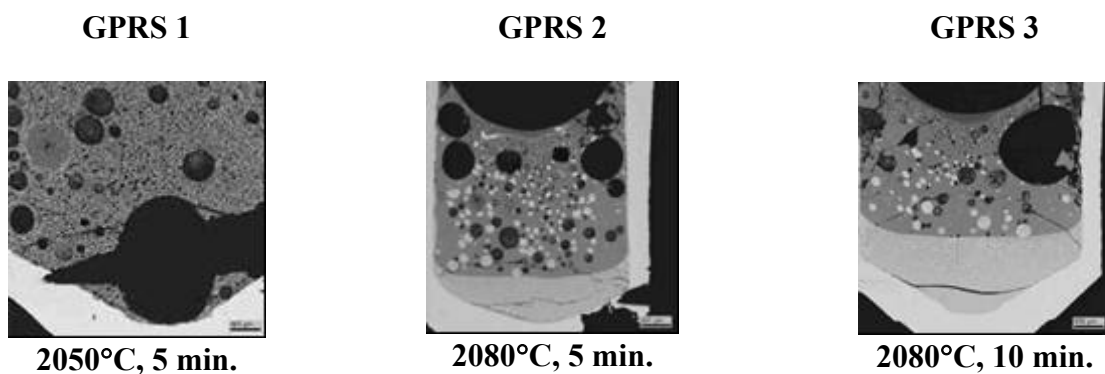
Fig. 2.22 – Macrophotographs of GPRS1-3 polished sections

SEM/EDX analysis of samples shows that the annealing temperature of 2050ºC is below monotectics. At 2080C the liquid stratifies, and if the exposition time at annealing is longer, the volume of heavy liquid grows.

- **Experiment GPRS4**

To determine the critical point of the miscibility gap the mixture was molten in a molybdenum crucible inside the Galakhov microfurnace; the melting was followed by quenching. Experimental conditions are given in Table 2.2.

- **Experiments GPRS 5-13**

To specify liquidus temperatures determined in experiments PRS 1-3 their compositions were annealed at different temperatures (experiments GPRS5-13) in the Galakhov microfurnace. Experimental matrix is given in Table 2.2.

ZrO_2-FeO_x system

To study phase equilibria in the ZrO_2-FeO_x system the high-temperature microscope was modernized. It was equipped with a spectral ratio pyrometer, which required a modification in the heating loop, because its area in the traditional model was not sufficient for the stable operation of pyrometer. The changed configuration of the heating loop required a higher capacity of the power source. The methodology of work with the modified high-temperature microscope was fine-tuned.

The initial compositions prepared by the sol-gel method and by the hydrothermal synthesis were examined by the visual polythermal analysis using the adjusted HTM. The studied compositions were controlled by MPCA (electron microscope ABT-55 equipped with a microproble device Link Analytical) and by EDRFA (ReSPEKT, analyzer of elemental composition). Table 2.5 gives the composition of specimens determined by different methods and objectives of specimen synthesis.

The sol-gel technology was also used in combination with hydrothermal synthesis. In this case in particular, hydroxide of iron (III) was precipitated in the suspension of ZrO_2 nanoparticles having the average size of approx. 20 nm, which had been produced by the method of hydrothermal dehydration of zirconium hydroxide. The composition of resulting specimens was also controlled by XRF and XRD (Table 2.6).

Table 2.5 – Compositions of specimens

ZrO_2	$FeO_{1.5}$		Objectives
mol.%			
90	10	By synthesis	Determine liquidus and solidus temperatures and compositions of solid solutions
86.7±0.6	13.3±0.6	EDX (Link)	
50	50	By synthesis	Determine miscibility gap boundaries
46.5	43.5	EDX (Link)	
25	75	By synthesis	Determine liquidus and solidus temperatures and compositions of solid solutions
23.6±0.6	76.4±0.6	EDX	
26.4±0.9	73.6±1.7	XRF	
5	95	By synthesis	Determine eutectic temperature and composition
5.8±0.4	94.2±0.4	EDX	
6.2±0.3	93.8±2.0	XRF	

Table 2.6 – Composition of specimens in accordance with XRF and EDX

Nano-sized ZrO_2	$FeO_{1.5}$		Objectives
mol.%			
25	**75**	By synthesis	Determine liquidus and solidus temperatures and compositions of solid solutions
28.9±0.6	71.1±0.6	EDX	
29.1±1.2	70.9±1.5	XRF	

A traditional technique was also used – mechanical mixing of oxides followed by their annealing at 1200°C during 4 and 6 hours and cooling in the furnace (Table 2.7).

Table 2.7 - Composition of specimens after mechanical mixing and annealing at 1200°C during 4 and 6 hours

ZrO_2	$FeO_{1.5}$		Objectives
mol.%			
5.3	94.7		Determine eutectic temperature and composition
11.1	88.9		
17.7	83.3		
25.0	75.0	By synthesis	Determine miscibility gap boundaries
33.4	66.6		
42.9	57.1		
53.9	46.1		
66.6	33.4		
81.8	18.2		Determine composition of solid solutions

Fe(OH)$_3$-ZrO$_2$ specimens produced by the sol-gel synthesis (Table 2.4) and combined sol-gel and hydrothermal synthesis (Table 2.5) were subjected to thermal treatment in the DTA mode followed by XRF (Figs. 2.23, 2.24) for evaluating the temperature of Fe$_2$O$_3$ formation at the dehydration of iron hydroxide and for determining phase composition of synthesized specimens.
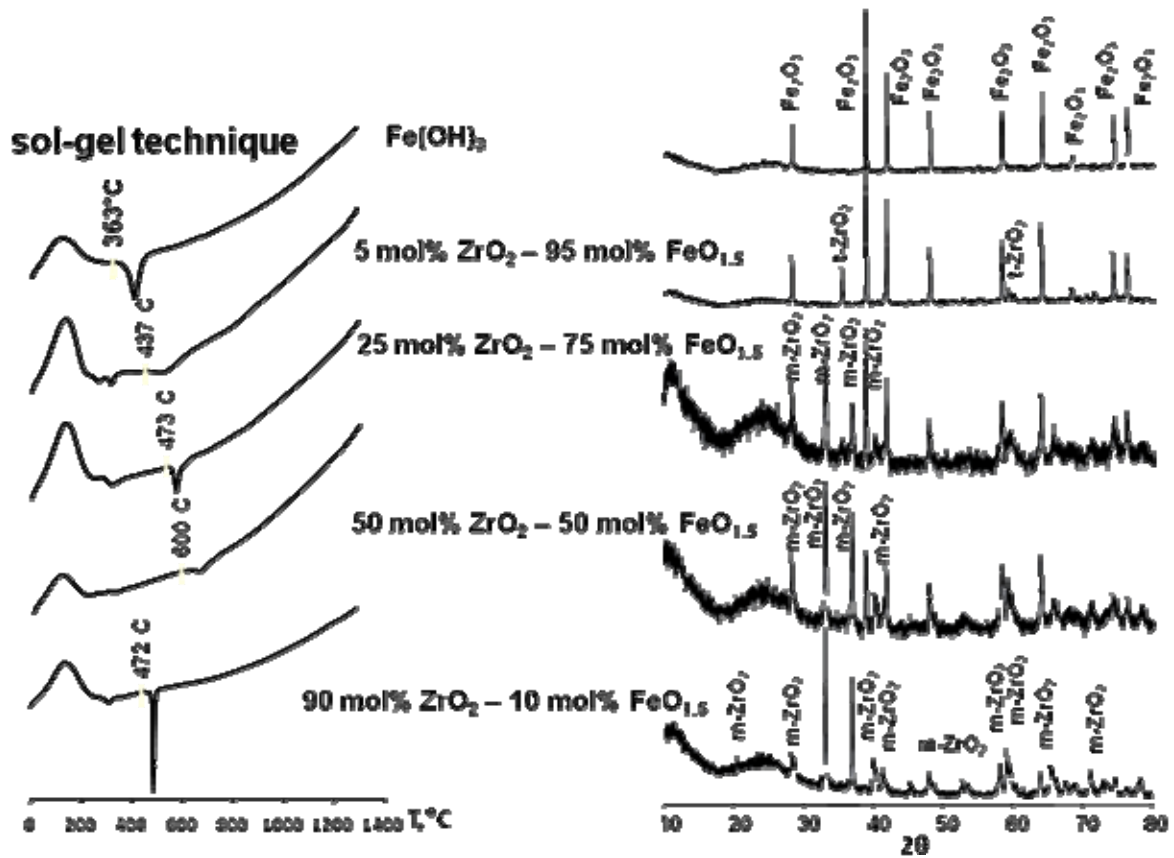
Fig. 2.23 – Results of diffrential thermal analysis followed by X-ray fluorescence analysis of compositions in the ZrO_2-FeO_y system of a corresponding composition produced by the sol-gel method
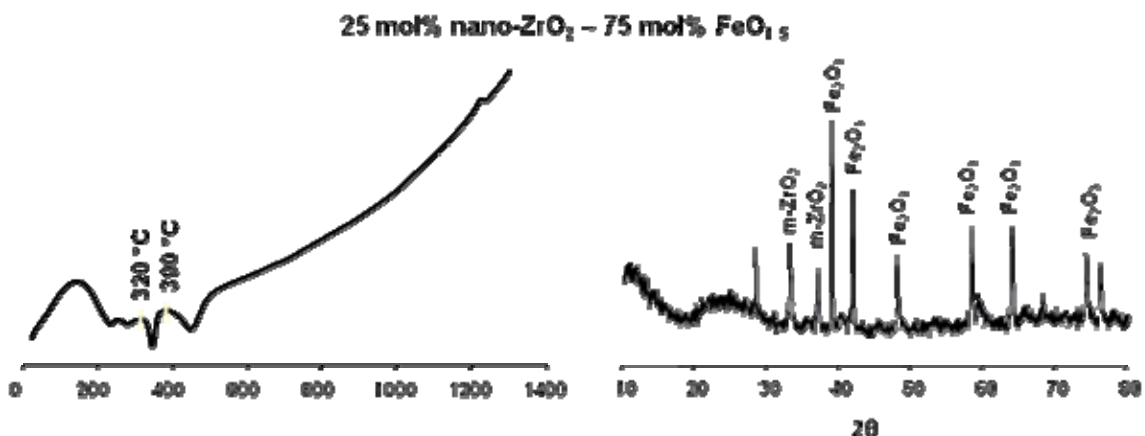

Fig. 2.24 - Results of diffrential thermal analysis followed by X-ray fluorescence analysis of compositions in the ZrO_2-FeO_y system of a corresponding composition produced by the combination of hydrothermal synthesis and sol-gel method

The analysis of new data brings a conclusion that the behavior of studied compositions at heating very much depends on the technique of their preparation. If we compare the behavior of specimens, which have the same composition, but different preparation methodologies, we can see different trajectories of curves (DTA curves) and a shift of peak, which indicates the Fe_2O_3 crystallization, to a lower temperature domain (Figs. 2.23 and 2.24). We also should note that an increase in the amount of zirconium oxide in the system causes the shift of iron oxide crystallization peaks to a high-temperature domain.

The XRF data have shown that in case of small content of zirconium oxide in the system (5 mol. %) during heating a formation of Fe_2O_3 as hematite and solid solution based on the ZrO_2 tetragonal modification is observed. An increase of ZrO_2 content in the system to 25 mol.%, and later to 50 mol.% results both in the formation of hematite (Fe_2O_3) and mostly monoclinic modification of ZrO_2 (t-ZrO_2 is found only in trace quantitative). If the composition corresponds to 90 mol.%, the X-ray diffractogram shows only m-ZrO_2 peaks. Such behavior can be explained only by the kinetic phenomena; it requires additional studies.

Initial compositions prepared by the sol-gel and hydrothermal synthesis methods were also studied by the visual polythermal analysis using the adjusted HTM.

Figs. 2.25-2.27 show the results of visual polythermal analysis of compositions. Each composition was studied by three experiments. The resulting data enable to make two main conclusions: registered temperature of spreading start in the ZrO_2-FeO_x system depends on the way the composition was prepared. In case of $Fe(OH)_3$ precipitation on ZrO_2 nanoparticles (Table 2.5) the visually registered temperature of spreading start was 50°C lower than for compositions produced by the sol-gel synthesis (Table 2.4). It can be explained by the structural stabilization of ZrO_2 and formation of solid solutions on its basis.

Along with the spreading start caused by the eutectic melting in the Fe_2O_3-Fe_3O_4-ZrO_2, system at approx. 1500°C the specimen shape degradation is observed, which is probably caused by the Fe_2O_3 transition into Fe_3O_4.

To determine the solidus temperature in the system and have a more detailed study of phenomena found by VPA, it is planned to conduct DSC and TGA at a higher temperature. T_{liq} was determined at the complete specimen spreading on the heater-holder. Table 2.8 gives VPA data taking into account the temperature measurement errors. Using the data of pre-experimental calibration tests the technical error can be evaluated as ±50°C.

Table 2.8 – VPA and HTM data in HTM

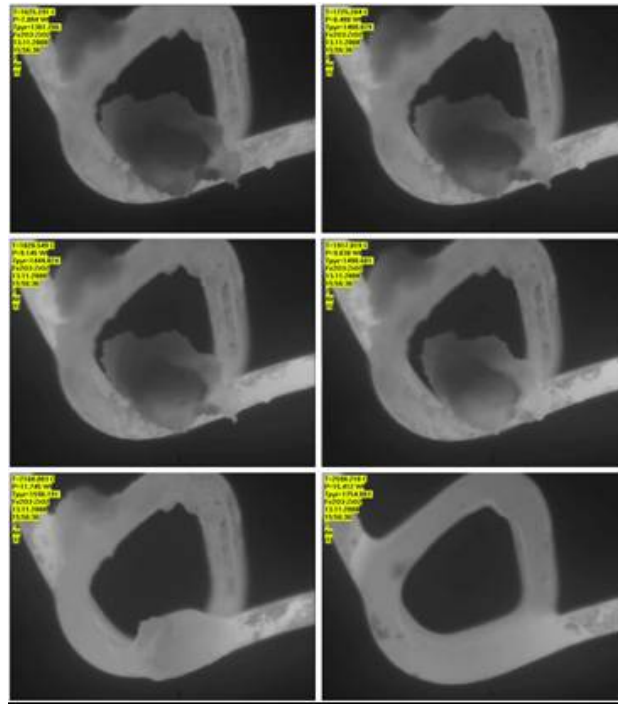| ZrO_2	$FeO_{1.5}$	Phase transition	T, °C
mol.%			
25	75	Fe_2O_3->Fe_3O_4	1442±4
		Solidus	1508±15
		Liquidus	1741±10
5	95	Fe_2O_3->Fe_3O_4	1411±28
		Solidus	1515±22
Nano-sized 25	75	Fe_2O_3->Fe_3O_4	1378±4
		Solidus	1489±4
		Liquidus	1780±25

Fig. 2.25 – Video fragments of VPA experiment in the high-temperature microscope (heating sequence). Composition 25 mol% ZrO$_2$ – 75 mol% FeO$_{1.5}$

Temperature of the specimen shape degradation – 1445°C

Temperature of the active spreading on the holder – 1495°C
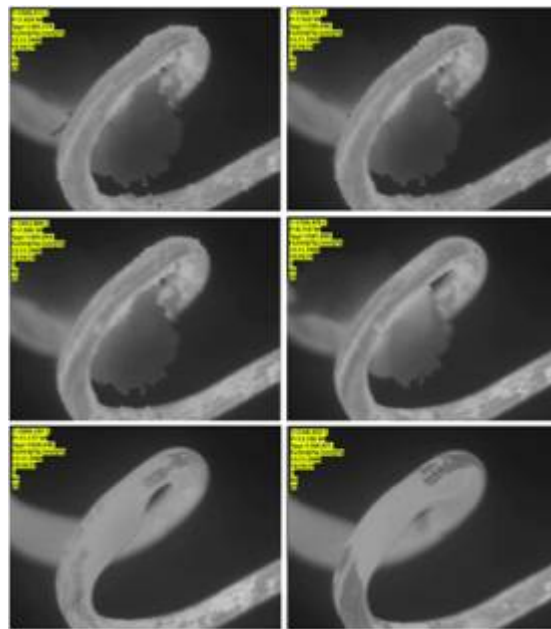
Temperature of complete spreading – 1755°C

Fig. 2.26 - Video fragments of VPA experiment in the high-temperature microscope (heating sequence). Composition 25 mol% nano-ZrO$_2$ – 75 mol% FeO$_{1.5}$

Temperature of the specimen shape degradation – 1395°C

Temperature of the active spreading on the holder – 1493°C

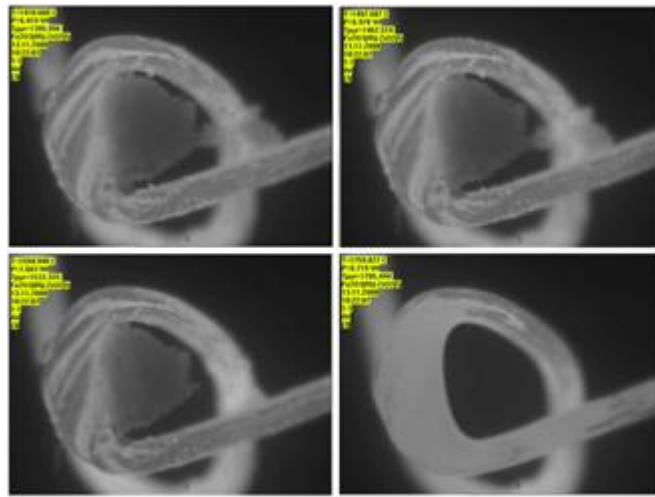Temperature of complete spreading – 1769°C

Fig. 2.27 - Video fragments of VPA experiment in the high-temperature microscope (heating sequence). Composition 5 mol% ZrO_2 – 95 mol% $FeO_{1.5}$.

Temperature of the specimen shape degradation – 1463°C
Temperature of the active spreading on the holder – 1533°C
Temperature of complete spreading – 1705°C

Figs. 2.28 and 2.29 show the specimen microstructures and compositions (SEM/EDX-analysis) after thermal treatment during heating in the high-temperature microscope.

Fig. 2.28. (Composition: 25 mol.% ZrO_2 – 75 mol.% $FeO_{1.5}$) shows the zone of eutectic crystallization (1 mol.% ZrO_2 – 88 mol.% $FeO_{1.5}$) and grains of primary crystallization –ZrO_2-based solid solution containing 14 mol.% FeO_y. There are zones, which correspond to FeO_y and do not contain ZrO_2, which indicates the absence of iron oxide-based solid solutions in the $ZrO_2 - FeO_{1.5}$ system. This can be confirmed by the analysis of phase structure and composition for mixture 5 mol.% ZrO_2 – 95 mol.% $FeO_{1.5}$ (Fig. 2.29). In this case the primary crystallization zones are iron oxide grains without anyZrO_2 admixture .
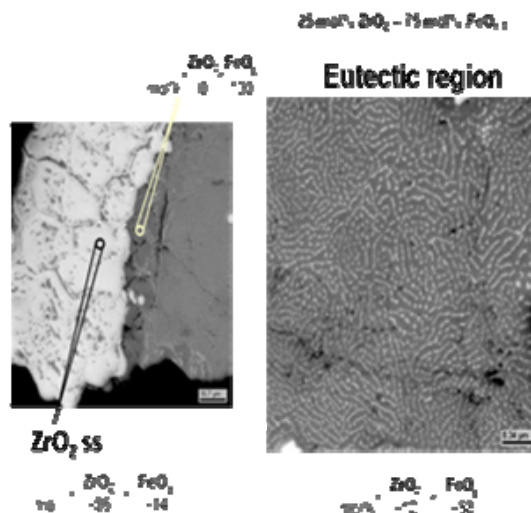

Fig. 2.28 - SEM/EDX analysis of composition 25 mol% ZrO_2 – 75 mol% $FeO_{1.5}$
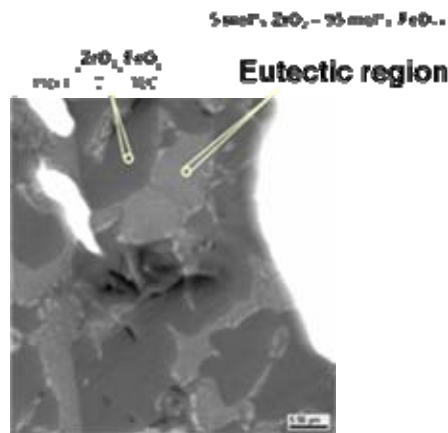
Fig. 2.29 - SEM/EDX analysis of composition 5 mol% ZrO_2 – 95 mol% $FeO_{1.5}$

To summarize: the completed studies have specified the eutectic composition of the ZrO_2-FeO_y system - ZrO_2-based solid solution composition at the eutectic temperature; FeO_y-based solid solutions have not been found. The results have been incorporated into the phase diagram (Fig. 2.30).
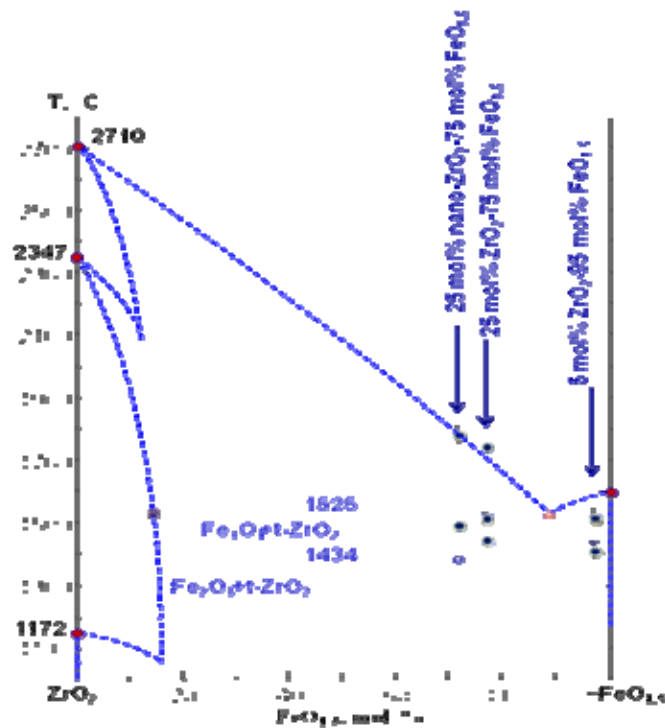

Fig. 2.30 – Phase diagram of the ZrO_2-FeO_y system in air

UO_2-CaO system

To study binary oxidic system UO_2-CaO the methods of VPA IMCC (PRS experimental series) and SEM/EDX were used.

Experiments PRS4-6 were performed on RASPLAV-4 experimental setup. Fig 2.1 shows the furnace schematics.

The matrix of PRS experimental series for the UO₂-CaO system is given in Table 2.9.

Table 2.9 - PRS experimental ser4rties for the UO$_2$-CaO system

Test	Content, mass.% / at.%	
	UO$_2$	CaO
PRS-4	82.8/50	17.2/50
PRS-5	4.6/1	95.4/99
PRS-6	50/17.2	50/82.8
	35.4/10.2	64.6/89.8

- **Experiment PRS-4**

In experiment PRS-4 three measurements of liquidus temperatures were made by the VPA IMCC and two melt samples were taken for the melt composition analysis. Fig. 2.31 shows pyrometer indications and anode voltage measured during the experiment. Figs. 2.32-2.34 show thermogram corresponding to the time of liquidus temperature measurements. After liquidus temperature was measured the close-to-equilibrium molten pool crystallization was carried out by the gradual shift of the pool from the inductor at the speed of 7.5 mm/h..
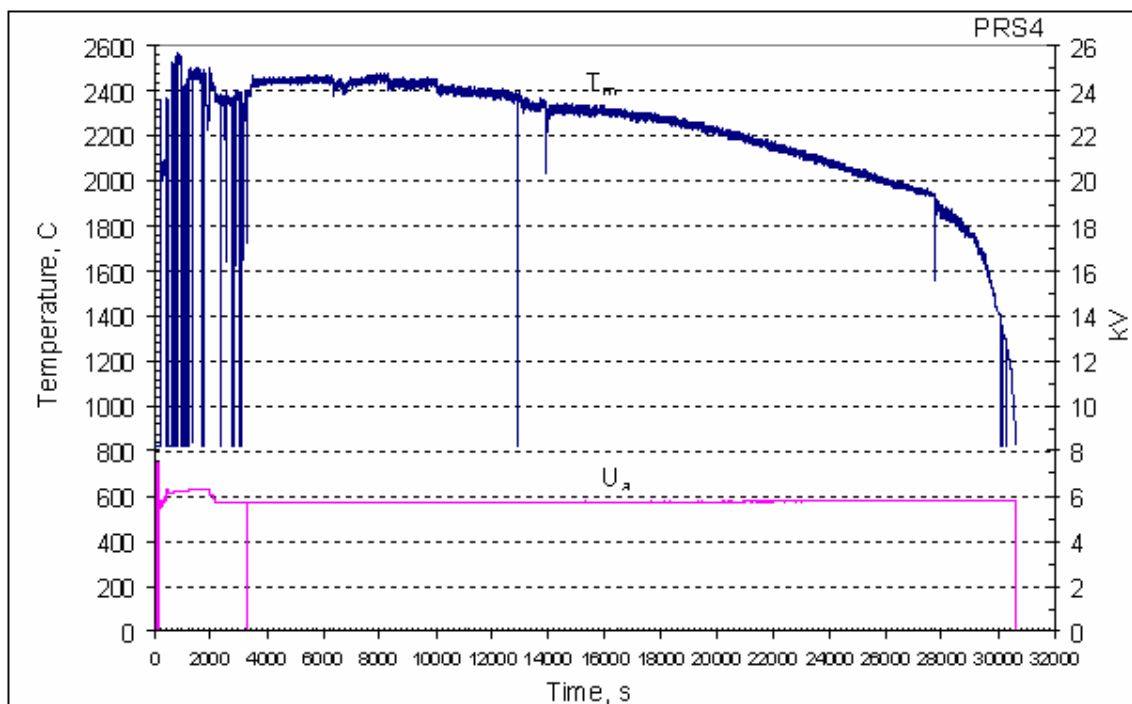

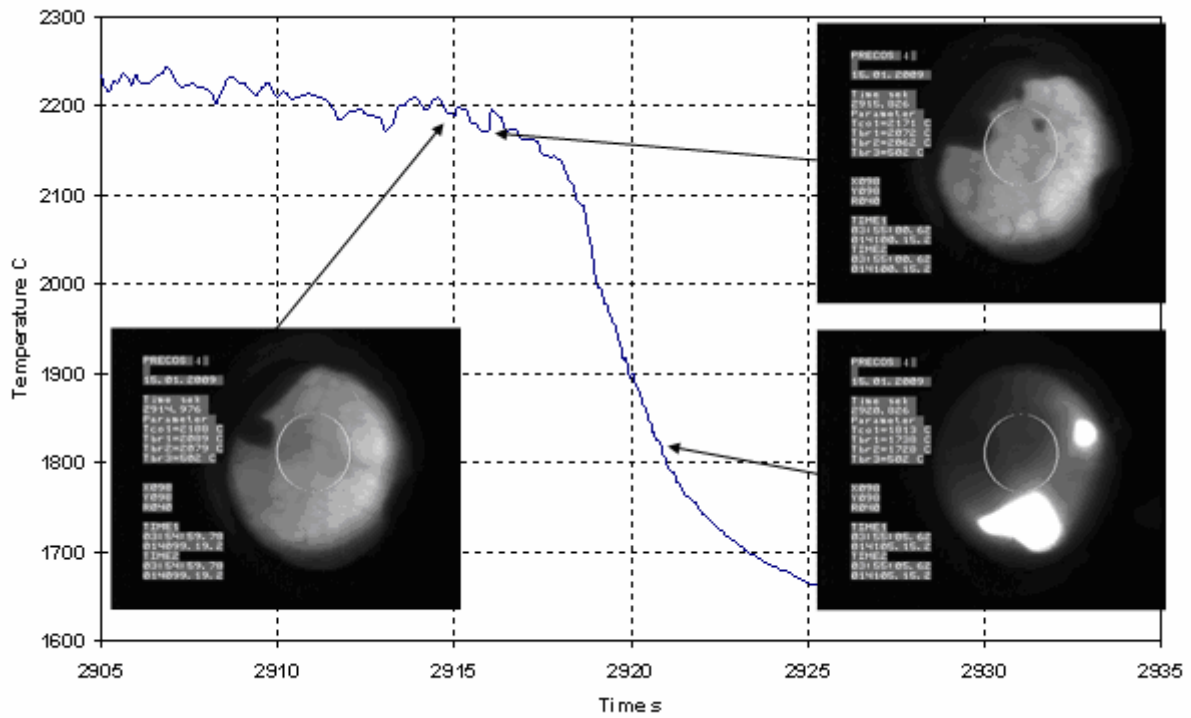**Fig. 2.31 – Dynamics of anode voltage (U$_a$) and pyrometer readings (T$_m$)**

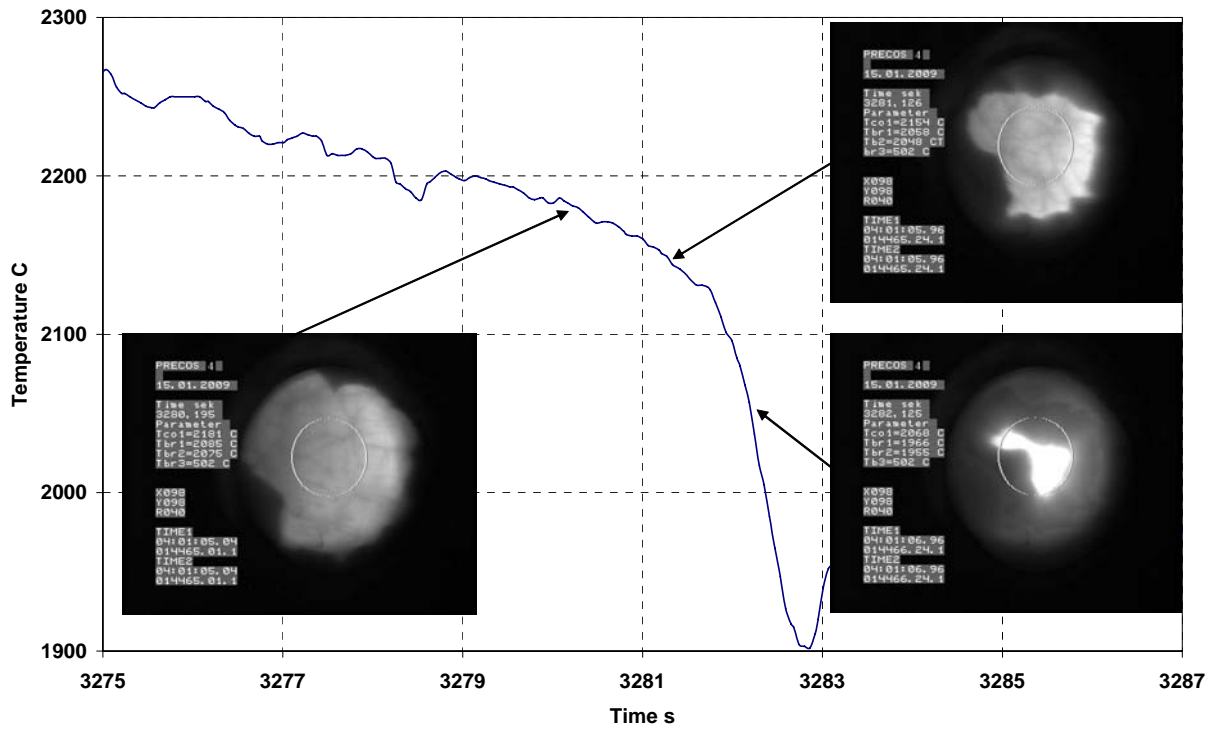**Fig. 2.32 – Thermogram fragment, experiment PRS-4**

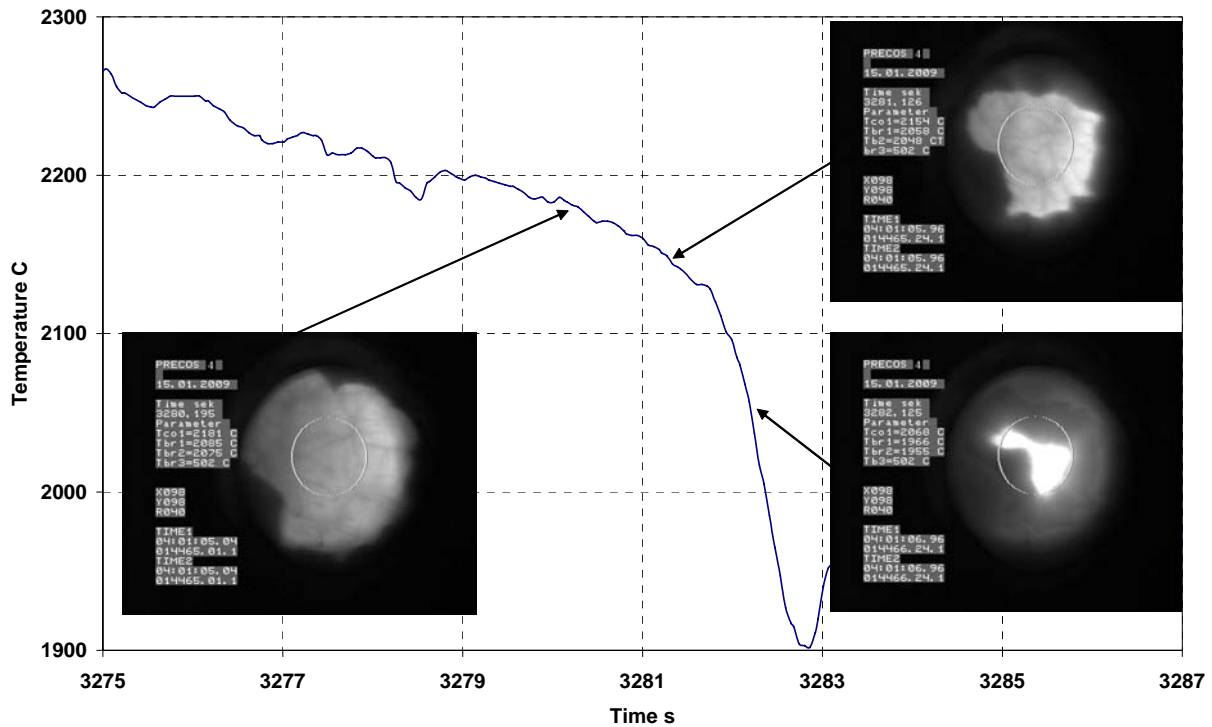**Fig. 2.33 - Thermogram fragment, experiment PRS-4**

Fig. 2.34 - Thermogram fragment, experiment PRS-4

T_{liq} for the three measured compositions is 2188, 2195 and 2181°C.

- **Experiment PRS-5**

In PRS-5 an attempt was made to measure the liquidus temperature near the CaO melting point. The startup heating was completed successfully. But the molten pool was not formed and measurements were not made due to a low electric conductivity of the melt. Current frequency of 5.28 MHz produced by RASPLAV-4 was not enough for maintaining this composition in a molten condition. A decision was taken to increase the concentration of uranium oxide in the next experiment.

- **Experiment PRS-6**

In PRS-6 two melt compositions were studied (Table 2.9) within one melting session. The second composition was produced by adding CaO into the molten pool. Fig. 2.35 shows pyrometer readings and anode voltage dynamics during the experiment. Two measurements of liquidus temperature were made in PRS-6 by VPA IMCC and two melt samples were taken to identify the first melt composition; one sample was taken and two liquidus temperature measurements were made after the CaO addition. Figs 2.36–2.39 show thermogram fragments at the time of liquidus temperature measurements.

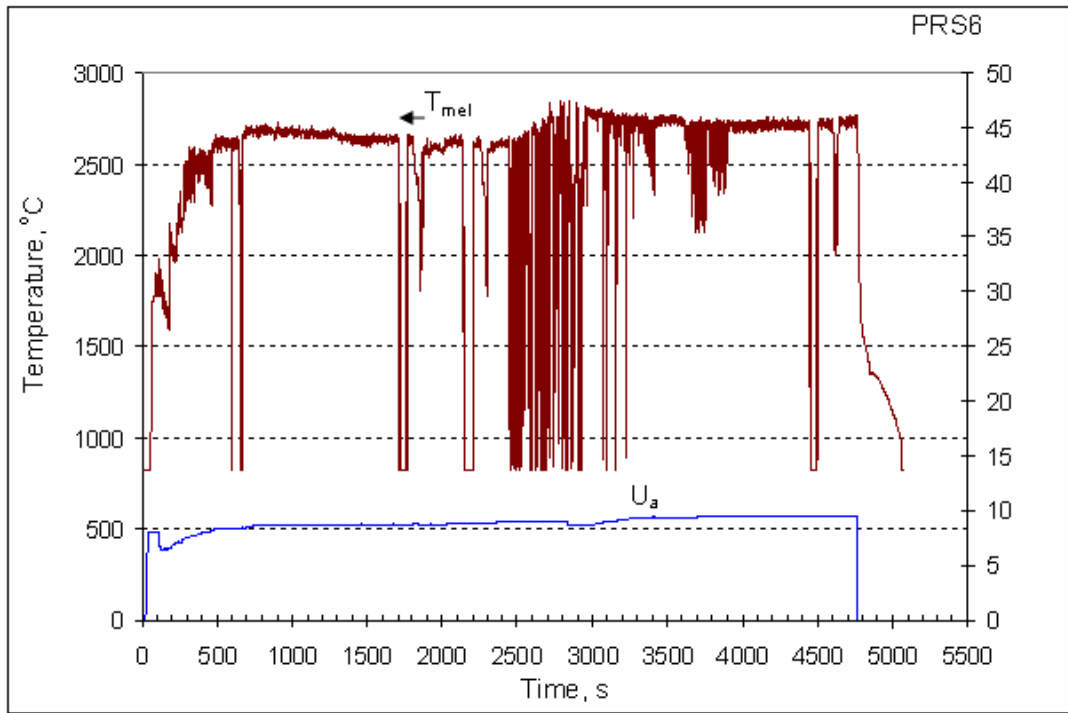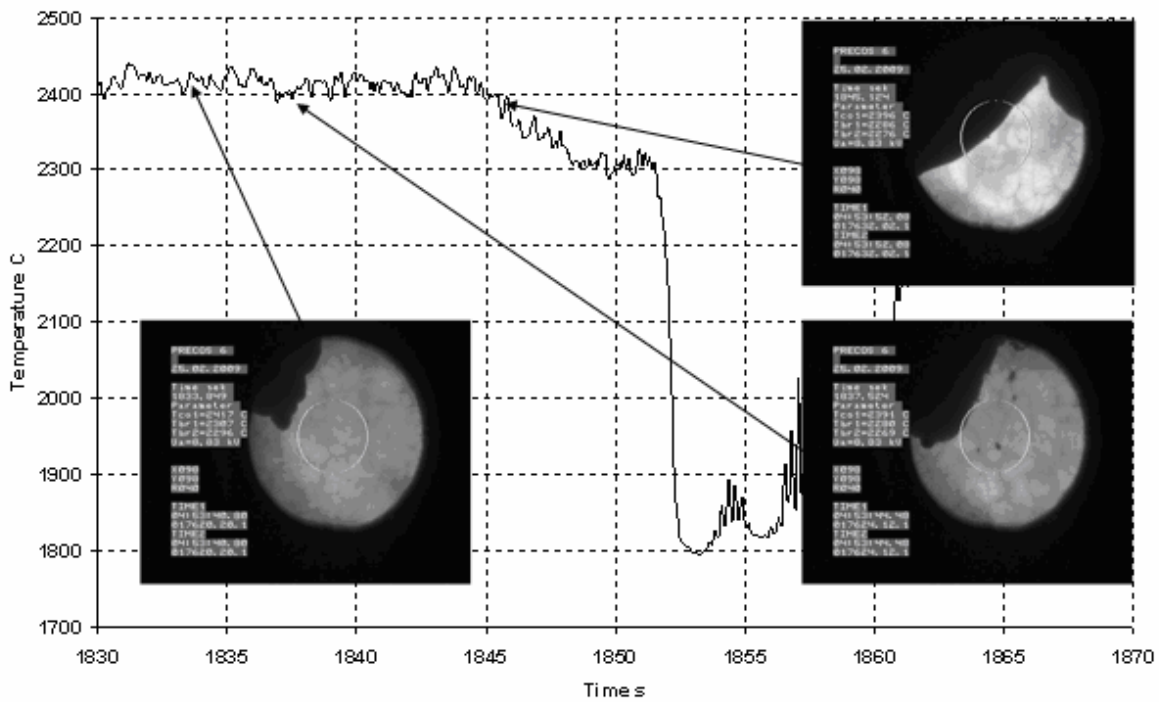**Fig. 2.35 – Dynamics of anode voltage (U$_a$) and pyrometer readings (T$_m$)**

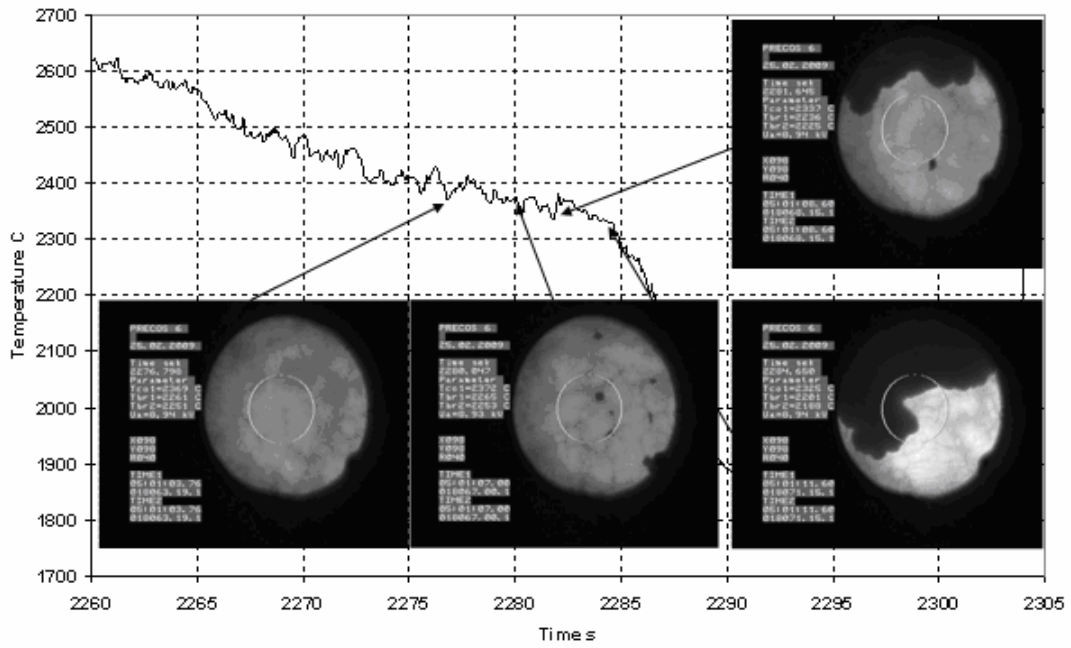**Fig. 2.36 - Thermogram fragment, experiment PRS-6**

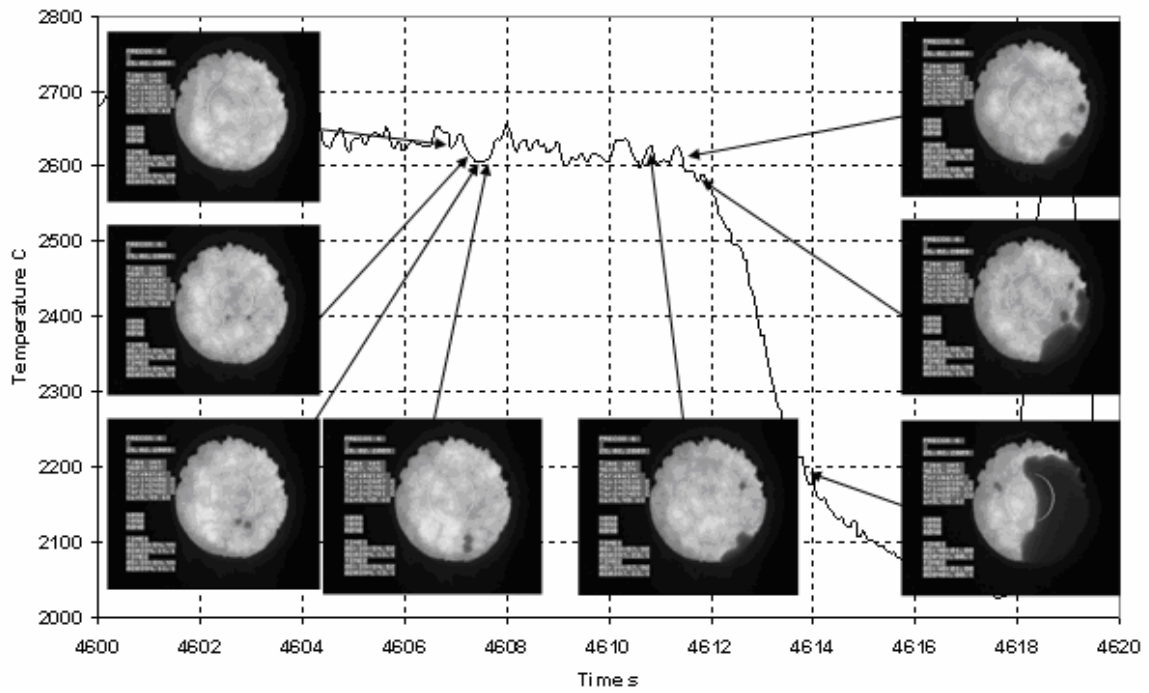**Fig. 2.37 - Thermogram fragment, experiment PRS-6**

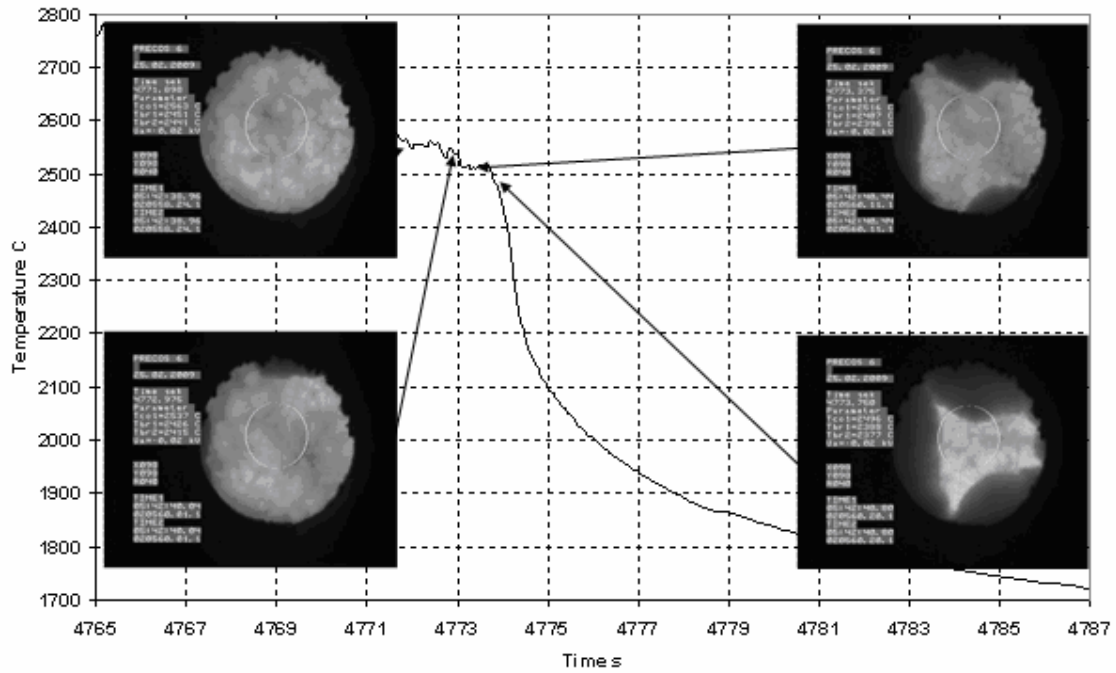**Fig. 2.38 - Thermogram fragment, experiment PRS-6**

Fig. 2.39 - Thermogram fragment, experiment PRS-6

Liquidus temperature measured for the first composition was 2417, 2370°C, and for the second – 2600, 2550°C.

Table 2.10 shows molten pool compositions measured by different methods; the measurements were made during the evaluation of liquidus temperature in the completed experiments.

Table 2.10 – Measured molten pool compositions

Test	Sample	Content from data, mol.%					
		ChA		EDX		XRF	
		UO_2	CaO	UO_2	CaO	UO_2	CaO
PRS-4	Sample #1	49.8	50.2	38.6	61.4	-	-
	Sample #2	48.7	51.3	39.2	60.8	51.4	48.6
PRS-6	Sample #1	26.09	73.91	17.2	82.8	26.0	74.0
	Sample #2	26.00	74.00	18.7	81.3	26.5	73.5
	Sample #3	17.74	82.26	12.0	88.0	17.0	83.0

Comparison of data provided by XRF and chemical analysis has shown their good agreement. The difference between XRF, ChA data and EDX is up to 12 at.%. A possible reason for such difference of XRF and ChA from the EDX data is in the preparation of samples. In XRF and ChA powders were used, which were prepared in the inert atmosphere, and had particle size below 50 μm. For EDX polished sections were prepared, which underwent additional dry polishing; and this could lead to UO_2 crumbling from the surface layer. It is planned to have a detailed investigation of the difference in the results.

Fig. 2.40 shows liquidus temperatures measured in all completed experiments of the binary system UO-CaO. Compositions are derived by averaging ChA and XRF data.
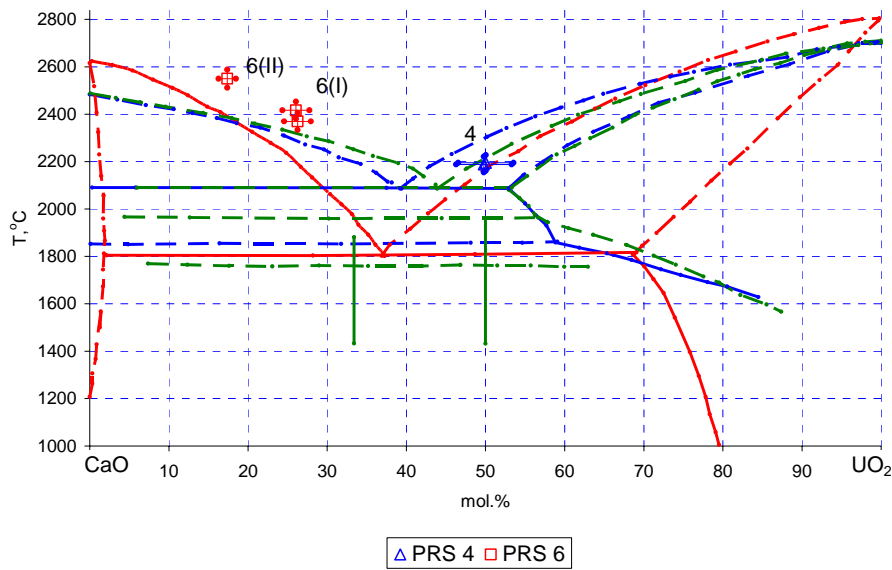
Fig. 2.40 – Comparison of first PRECOS data with different versions of the UO_2-CaO phase diagram [5, 6, 7]

From first results on this system it can be assumed that melting temperature of pure CaO is considerably higher than values given in [5 - 7], respectively, and liquidus line from the CaO side from eutectics is higher than in all published versions of this phase diagram.

Table 2.11 gives recommended experimental values on liquidus temperatures of different compositions.

Table 2.11 – Recommended liquidus temperatures for melt compositions in PRS-4,6 experiments

Test	Sample No	Content, mol.%		T_{liq}, °C
		UO_2[1]	CaO	
PRS-4	**Sample #1**	49.80±3.5	50.20	2188±33
	Sample #2	50.05±3.5	49.95	2195±33
PRS-6	**Sample #1**	26.05±1.7	73.95	2417±36
	Sample #2	26.25±1.7	73.75	2370±36
	Sample #3	17.37±1.1	82.63	2550±38

[1] averaged from XRF and ChA.

Conclusions

– Experimental studies were preceded by the analysis of published data on binary systems

– For the experimental studies the equipment was modernized and experimental techniques were adjusted

– Experiments on the Zr- O systems were completed, as well as PRS 1-8 and GPRS 1-14 series in the $UO_2 – SiO_2$, $UO_2 – CaO$ systems. Studies of the $ZrO_2 - FeO_y$ system were completed. Their results are processed.

- − First results revealed a necessity to specify the CaO melting temperature, coordinates of eutectic point and final solubility of uranium oxide in the calcium oxide at the eutectic temperature.

References

1. P.-Y. Chevalier, E. Fischer, B. Cheynet. "Progress in the thermodynamic modeling of the O-U-Zr ternary system." // Computer Coupling of Phase Diagrams and Thermochemistry 28 (2004) P. 15-40.
2. Jones T.S., Kimura Sh., Muan A. // J. Amer. Cer. Soc. 1967. V.50, N 3. P.137-142.
3. Petrov Yu.B., Udalov Yu.P., Slovak J., Morozov Yu.G. // Glass Physics and Chemistry. 2002. V. 28, N 3. P. 139–146.
4. Bechta S.V., Krushinov E.V., Almjashev V.I., Vitol S.A., Mezentseva L.P., Petrov Yu.B., Lopukh D.B., Khabensky V.B., Barrachin M., Hellmann S., Froment K., Fisher M., Tromm W., Bottomley D., Defoort F., Gusarov V.V. // J. Nucl. Mater. 2006. V.348, 114-121.
5. O,V. Almiasheva. Hydrothermal synthesis, structure and properties of nanocristals and nanocomposites in the ZrO$_2$-Al$_2$O$_3$-SiO$_2$ system: Abstract of a thesis for Doctor's degree in chemistry / ISCh Ras. St. Petersburg. 2007. 24 c (in Russian).
6. Alberman K. B., Blakey R.C., Anderson J. S. // J. Chem. Soc. 1951. N5. P. 1352-1356.
7. Amato I. // Metallurgia ital. 1966. An. 58, N 9. P.365-368;
8. Holc J., Kolar D. // J. Solid State Chem. 1986. Vol. 61, N 2 P. 260-262.

3. Current technical status

- Activities are carried out in accordance with schedule

4. Cooperation with foreign collaborators

Foreign collaborators within the project are well-known experts representing EU scientific research centers:

1. Dr. Marc Barrachin), France
   IRSN/DRS/SEMAR/CEN Cadarache
2. Dr. Fransoise Defoort, France
3. Dr. Alexei Miassoedov, Germany
   Forschungszentrum Karlsruhe GmbH, IKET
4. Dr. David Bottomley, Germany
   EUROPAISCHE KOMMISSION, Institut fur Transurane (ITU)
5. Dr. Pascal Piluso, France
   CEA Cadarache – DEN/DTN/STRI
6. Manfred Fischer, Germany
   AREVA NP GmbH
7. Dr. Sieghard Hellmann, Germany
   AREVA NP GmbH

The Project is implemented in close cooperation with foreign collaborators, in particular the joint activities are: detailed discussion and approval of Work Plan and experimental matrix; analysis and evaluation of results of each experiment; introduction of updates into the experimental specifications; numerical analyses carried out in parallel; preparation of joint papers and contributions into conferences.

The scope of PRECOS work and its results were discussed at joint meetings with collaborators:

- First meeting of the PRECOS Steering Committee with collaborators was held on 10 July 2008 in St. Petersburg.
- Second meeting of the PRECOS Steering Committee with collaborators was held on 26 May 2009 in St. Petersburg.

During the reported year the Project contractors took part in the meeting of CEG-SAM expert team: at 14 CEG-SAM meeting 9-11 September 2008 in Kiev, Ukraine and at 15 CEG-SAM meeting, 9-13 March 2009, Villigen, Switzerland. The completed studies within the Project were reported there.

Two papers and a presentation at an international conference have been prepared jointly with collaborators

5. Problems encountered and suggestions to remedy

There are organizational problems related to the licensing of the ITES OIVT RAS laboratory on handling uranium-bearing specimens. The following has been done to resolve the problem:

1) Requirements to the laboratory room have been determined.
2) The room has been found (an agreement with an institution authorized on such work is formulated).
3) Terms of reference have been prepared.
4) An approval from the RAS Presidium has been received.
5) The chosen room have been chosen and a list of requirements to it has been prepared.
6) Personnel training has been completed.
7) Medical examination of the personnel has been made.
8) A design project of the room has been made by the authorized organization (NPO Lutch).
9) Room repairs have been completed. The room is equipped with the required technical and auxiliary systems. A separate room for the storage of radioactive waste has been arranged.
10) Means of personal dosimetry control have been prepared
11) An expert institution authorized on the room expertise has been contacted.

Necessary to:

1) Get official expert conclusion on the room design.
2) Get official conclusion on the room suitability.
3) Provide radiological control means.
4) Compile technical documentation.
5) Get permit from the sanitary authority (regulator) to use radioactive sources (RS).
6) Prepare the technical documentation package.
7) Get a license on RS handling.

6. Perspectives of future developments of the research/technology developed

In accordance with Work Plan